AD-783 304

A DEEP HOLE STRESS MEASUREMENT DEVICE

Earl R. Hoskins, et al

South Dakota School of Mines and Technology

Prepared for:

Air Force Office of Scientific Research

10 July 1974

IDENTIFICATION

ARPA Order No.: 1584 Amend. No. 4

Program Code No.: 2F10

Name of Contractor: The South Dakota School of Mines and Technology

Effective Date of Contract: 01 March 1972

Amount of Contract: $80,674.00

Contract No.: F 44620-72-C-0029

Principal Investigators: Earl R. Hoskins and Edwin H. Oshier

Telephone No.: (605) 394-2345

Short Title: Development and Field Testing of a Deep Hole Stress Measurement Device

14 KEY WORDS	LINK A		LINK B		LINK C	
	ROLE	WT	ROLE	WT	ROLE	WT
In Situ Stress						
Residual Stress						
Rock Mechanics						

Security Classification

DOCUMENT CONTROL DATA - R & D AD 783304

(Security classification of title, body of abstract and indexing annotation must be entered when the overall report is classified)

1 ORIGINATING ACTIVITY (Corporate author)

South Dakota School of Mines & Technology
Department of Mining Engineering
Rapid City, South Dakota 57701

2a. REPORT SECURITY CLASSIFICATION

Unclassified

2b. GROUP

3 REPORT TITLE

A Deep Hole Stress Measurement Device

4 DESCRIPTIVE NOTES (Type of report and inclusive dates)

Scientific Final

5 AUTHOR(S) (First name, middle initial, last name)

Earl R. Hoskins
Edwin H. Oshier

6 REPORT DATE	7a. TOTAL NO. OF PAGES	7b. NO. OF REFS
July 10, 1974	142	28

8a. CONTRACT OR GRANT NO	9a. ORIGINATOR'S REPORT NUMBER(S)
F44620-72-C-0029	102
b. PROJECT NO	
c. AO 1584 Amend. No. 4	9b. OTHER REPORT NO(S) (Any other numbers that may be assigned this report)
d.	AFOSR - TR - 74 - 1235

10 DISTRIBUTION STATEMENT

Approved for Public Release: Distribution Unlimited

11 SUPPLEMENTARY NOTES	12. SPONSORING MILITARY ACTIVITY
TECH.	Air Force Office of Scient. Res. 1400 Wilson Boulevard (NPG) Arlington, Virginia 2209

13 ABSTRACT

This report describes the work done on the development of a deep hole stress measurement device under Contract No. F44620-72-C-0029. Our intention was to field test the device, however, we did not get that far. In this report we describe the mechanical design, the development of the telemetry and control systems, and the considerable effort spent on studying the problems associated with residual stresses in in situ rocks and their effects on stress measurement techniques. Data reduction from the device has also received a great deal of attention. Three different approaches were tried and these are also described in the report.

DD FORM 1 NOV 68 1473

Security Classification

Table of Contents

Table of Contents (cont.)

List of Tables

List of Figures

List of Figures (cont.)

I SUMMARY

This report describes the work done on the development of a deep hole stress measurement device under Contract No. F44620-72-C-0029. Our intention was to field test the device, however, we did not get that far. In this report we describe the mechanical design, the development of the telemetry and control systems, and the considerable effort spent on studying the problems associated with residual stresses in in situ rocks and their effects on stress measurement techniques. Data reduction from the device has also received a great deal of attention. Three different approaches were tried and these are also described in the report.

II. Introduction

The purpose of this investigation was to develop, build and test an instrument to accurately measure primary rock stresses in the side walls of long (1000 meters or more) 6½ inch diameter drill holes. This instrument would be used to measure stresses around existing uncased oil field holes. In particular we wanted to be able to make this instrument available for projects such as the Rangely, Colorado, Oil Field Earthquake Investigation. In this and other earthquake investigations one of the most important missing bits of information required for complete analysis of the problem is the existing primary state of stress in the ground. Other potential areas of application for our instrument include: site investigations for nuclear power plants, determining suitability of a site for underground nuclear testing, investigating an underground location as a potential storage cavern for L. N. G. (liquefied natural gas), site investigations for major tunnels and underground power houses, and planning studies for deep underground mines. At the present we know of no existing technique or apparatus which can accurately determine the three principal stresses that are acting and their orientations in long drill holes.

State of the Art

Numerous rock stress measurement techniques have been

developed based on the principle of strain relief. The general idea is that the rock is believed to be under some initial stress. Some of the rock is removed and deformation of the remaining rock occurs. The deformation is measured and recorded. Usually the next step is to make the assumption that the rock is isotropic and linearly elastic. If the geometry of the strain relief system is simple enough, an analytical solution based on the assumptions of linear isotropic elasticity is found. This solution relates primary or field stresses to the strains in the rock where the deformation was measured through the elastic moduli of the rock. The moduli are determined by laboratory tests on samples of the rock and these moduli along with the measured strains and/or deformations are put into the equations of the analytical solution and the equations are solved for the primary stresses.

If the geometry of the system is too complicated for an analytical solution to be found there are still three methods of getting the primary stress-strain at the measuring position relationship: (1) a numerical approximation can be made using finite difference of finite element techniques. This procedure is usually limited in practice to two-dimensional analyses because of limitations on the size of the available computers; (2) a three-dimensional frozen

stress photoelasticity model is made and analyzed. The major criticism of this method is that Poisson's ratio in the model material is 0.50 whilst in rock it is commonly around 0.20; and (3) full scale laboratory calibration tests can be made in large blocks of rock with known stresses applied by a loading frame.

Several different techniques have evolved in the past 20 years for making strain relief stress measurements. These techniques differ from each other only in the details of (1) how they make the deformation or strain measurement, (2) how the measuring components are arranged relative to the strain relieving activity, and (3) just how the strain relief is accomplished. Two of the most widely used techniques are the borehole deformation gage and the borehole-end strain relief methods or "doorstoppers."

Both borehole deformation gages and "doorstoppers" have been extensively tested in the laboratory and successfully used in the field. There are many advantages and disadvantages claimed for each technique but the main problem with either of them is that the maximum depth of hole that they can practically be used in is of the order of 50 to 100 feet. Another disadvantage common to both techniques is that a drilling rig must be set up on the site and special holes drilled for the in situ stress determinations.

Another candidate technique for deep hole in situ stress measurements is hydraulic fracturing. Hydraulic fracturing is a technique originally developed to stimulate production from oil wells. A section of a borehole is sealed with straddle packers and fluid pressure is then applied to the bare walls of the hole between the packers. The pressure is increased until a fracture develops in the wall and the fracture propagates outwards as the fluid flows into it. Propagation is perpendicular to the direction of the minimum principal stress, and the fluid pressure required to extend the fracture is approximately equal to the minimum principal effective stress in the rock. This direct measure of the minimum principal stress is independent of rock properties.

Kehle (1964) has given a more refined analysis to determine the fluid pressure required to <u>initiate</u> a fracture in rock around a circular borehole. This analysis is based on the usual assumptions that the rock is elastic, isotropic, and homogeneous. In addition the rock must not be jointed or faulted. Fairhurst (1968) has used this analysis to attempt to determine all three principal stresses and their directions from carefully conducted hydraulic fracture tests and subsequent observations of the orientations of the fractures that were formed. Hydraulic fracturing can be done in holes of any depth, and it can be done in any

existing open (uncased) hole. The principal limitation of the technique is that it is difficult in practice to get much more than a single (the minimum) principal stress magnitude from the field measurements. Haimson (1973) and (1974) and Healy, et. al. (1974) have given recent examples of stress determination by hydraulic fracturing techniques.

The technique which we have attempted to develop in this project is based on the strain relief principal but is one which should be able to be used in existing uncased holes of any depth. We have run into several unexpected problems in the course of this research and are not nearly as far along as we had proposed or intended to be at this time. We have not yet run into insurmountable problems, however, and we do intend to continue working on the technique until it is a reliable field stress logging tool.

General Description of the Apparatus

We have designed, built and laboratory tested a device capable of determining the complete state of stress in the ground from measurements made in the side walls of 6 to 7 inch diameter, uncased oil field holes. The principle we use is strain relief undercoring using friction bonded strain gages. This technique was first proposed by Hoskins (1968) for use at the end of long but smaller (2 to 3 inch) diameter boreholes. In a 6 to 7 inch hole there is enough room to make

the measurements in the borehole walls and this is a considerable advantage. No borehole end preparation is required and stresses can be determined at various depths in the hole by repeated tests.

The principle of strain relief stress measurements by drilling a small hole in the center of a strain gage rosette, or trepanning, is well established and has been widely used in experimental stress analysis (c.f. Hetenyi, Handbook of Experimental Stress Analysis 1950). Hoskins (1968) has previously experimentally determined stress concentration factors for interpreting results of this type of test at the flattened end of a borehole. The same sort of experiments were done as a part of this project for tests performed in the walls of a borehole. Since an elasticity solution exists for the stresses in the walls of a cylindrical hole in a general three-dimensional stress field, only the effects of the strain gage rosette and trepanning drill geometry have had to be determined. Careful but straight-forward laboratory experiments were required.

Based on the requirements outlined in the introduction and the principal investigator's previous experience with other in situ stress and strain measuring devices we adopted the following set of specifications.

Resolution: 10 ppm strain - equivalent to approximately 3 bars in rock with a modulus of 3×10^5 bars

Operating Depth: 2500 meters

Hole Diameter: $6\frac{1}{2}$ inches $\pm \frac{1}{2}$ inch

Maximum Temperature: $100^{\circ}C$

Case Material: Stainless Steel (416)

Orientation: Sperry Sun Magnetic Device

Case Size: $5\frac{1}{2}$ inches diameter

Hydraulic Power: Bled from self-contained intensifier

Electrical Power: From self-contained battery pack

A general schematic of the apparatus is shown in Figure 1.

III. Mechanical Design

A brief description of the apparatus follows. There are three strain rosette trepanning units. They are mounted on hydraulic cylinders 120° apart about the longitudinal axis of the device. There are six other hydraulic shoes, three above and three below the measurement units to firmly fix the entire device in the hole. The hydraulic pressure is generated in the downhole apparatus and controlled from the surface. Rotation and advance of the trepanning drills is done by small electric motors also contained in the device

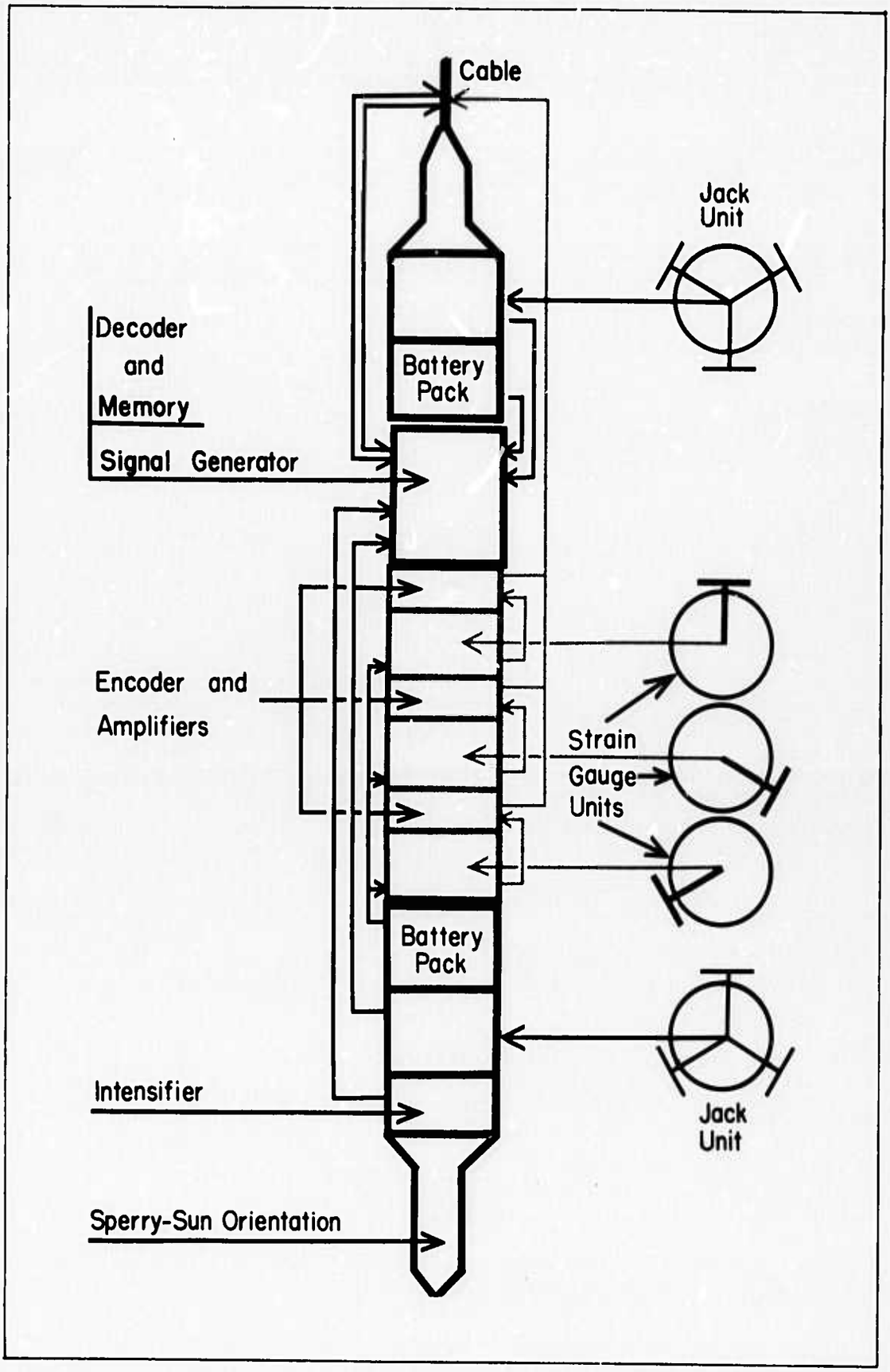
Cable
Jack Unit
Decoder and Memory
Battery Pack
Signal Generator
Encoder and Amplifiers
Strain Gauge Units
Battery Pack
Intensifier
Jack Unit
Sperry-Sun Orientation

but controlled from the surface. The entire apparatus is constructed as a waterproof bomb so that the electric motors and the data transmission package are operating in a dry environment. The strain gage signals will be fed up a cable to the surface and recorded on standard equipment. Power to the drilling motors and hydraulic pumps comes from a self-contained battery pack. A standard borehole surveying instrument will be fixed to the stress measurement device to indicate the orientation of the strain gages relative to geographical coordinates. A major feature of this system is that no drilling rig or derrick is required over the hole, only a wire line truck carrying the cable reel, power supplies, and read out instrumentation. We will not have to try to transfer signals up or down a rotating drill string.

The main portion of the apparatus was machined from 416 stainless steel bar stock. Design emphasis was placed on simplicity for the machine shop and extreme overall ruggedness of the final package.

Friction Bonded Strain Gages

The friction bonded strain gages are the most crucial element in the entire device. It was necessary for us to design and fabricate our own gages because the commercially available gages (Model CBF-6 manufactured by Tokyo Sokki Kenkyujo Col, Ltd.) could not be bent to conform to the

curvature of the sides of the borehole or adequately waterproofed. Several different versions of the friction bonded gages were constructed and tested. The best so far in terms of both performance and ease of construction is a composite consisting of 3 nylon plugs 3/4 of an inch diameter set into a steel holder with a backing plate. The strain gages are bonded to the nylon plugs with their leads fed through the backing plate into the main body of the apparatus. The outer surface of the gages is coated with a thin layer of 60 grit carborundum powder in an epoxy matrix. This outer surface will be in contact with the side walls of the borehole.

Telemetry and Control System

Telemetry System

The telemetry package, except for strain gauges and instrumentation amplifiers was supplied by IED, a division of Conic Corporation, San Diego, California. The system is capable of accepting 16 channels of analog data and converting them to digital form for transmissions to the surface on two wires of the seven conductor cable. At the surface the decoder drives a digital printer.

Control System

The control system is a digital system actuated by a 5-position Command Selector Switch. The commands are: Telemetry power, Jacks Out/In, Strain gauge Jacks Out/ In, Drill power, and Drill Out/In. The command signals are encoded in binary form and sent over 4 wires of the cable to the downhole decoder and memory unit. This unit contains a decoder and various relays which supply power to the appropriate control valves and to the electric drill and telemetry system. These power signals are also sent to the Status Signal Generator which sends a suitable status signal to a status light on the surface.
A pressure transducer is used to sense pressure variations resulting from the operation of control valves for Jacks Out, Strain Guage Jacks Out, and Drill Out.

IV Residual Stress Problems

Any in situ stress measurement technique actually measures the sums of several independent stress fields that are present. These independent stress components include: (1) the stress component due to gravity, (2) stresses due to thermal gradients, (3) the stress component due to the penetration of the rest of the stress field by the emplacement hole and measurement device, (4) the stress component due to currently active tectonic processes, and (5) the stress component due to locked in or residual stresses. In order to make intelligent use of the in situ measurements we have to be able to separate these various stress fields and report them independently. The vertical component of the gravity stress is known as well as the density of the rock, the vertical depth below a free surface, and the gravitational constant are known. It can be calculated from equation (1):

$$\sigma_v = \rho g h \qquad (1)$$

Where σ_v is the vertical stress due to gravity, ρ is rock density, g is the gravitational constant and h is the depth of the measurement below the free surface. The horizontal component of the gravity stress field depends upon material properties and material behavior as well. If the rock is considered to be homogeneous, isotropic and linearly elastic, the horizontal components of the gravity stress field are equal and can be calculated by equation (2):

$$\sigma_H = \left(\frac{\nu}{1-\nu}\right)\sigma_V \qquad (2)$$

Where σ_H is the horizontal stress due to gravity, ν is

Poisson's ratio and σ_v is the vertical stress due to gravity. Since rocks commonly have Poisson's ratios of 0.20 to 0.25 this equation leads to the usual estimate of the horizontal stresses being equal to 1/4 to 1/3 of the vertical stress.

Stresses due to thermal gradients can likewise be calculated from conventional thermo-elastic relationships if the magnitude of the gradients and the appropriate physical constants are known.

The laboratory and theoretical studies normally performed to prove any stress measurement device before it is taken into the field include determination of the secondary stress field due to the measurement technique itself.

We are left then with tectonic and residual stresses to determine separately. So far as we know there are as yet no published results of in situ measurements which accomplish this separation.

The tectonic stress field cannot be accurately calculated at our present stage of understanding of tectonic processes. In fact it is the tectonic component that we are usually attempting to determine when we make in situ measurements.

The residual stress field is here defined as the stress field remaining in a specimen in the absence of thermal gradients in the specimen or external loads applied to its boundaries. This is a standard definition of residual stress as used in metallurgical and ceramic engineering practice. Obviously the body must satisfy internal and external equilibrium and the integral of stresses taken over the volume of the body must equal zero.

While residual stresses in metals have long been known, routinely measured, and manipulated it is only in the past few years that they have received any detailed attention by workers in the field of rock mechanics. Since their magnitudes can approach the yield strength of the material they cannot be dismissed as of trivial importance. In fact, some of the high in situ stress values reported from surface measurements in supposedly stable or shield areas may be mainly residual with little or no tectonic component. Further, since the blocks of rock which we are using to laboratory calibrate our deep hole device do in fact contain significant residual stresses as does the Weber sandstone which is the reservoir rock at Rangely, Colorado, it is quite important that we become able to distinguish residual from tectonic stresses. Accordingly we have devoted considerable time and effort to the study and measurement of residual stresses in various rocks in the laboratory as a part of this project.

The initial experimental work was reported in the Final Report on Contract No. F44620-70-C-0073 entitled "Development of a Deep Hole Stress Measurement Device". Some additional experimental work, a discussion of the mechanism of formation of residual stresses, and a preliminary attempt at numerically modeling residual stresses have been performed during the present contract. The work was reported in paper by J.E. Russell and E.R. Hoskins at the 14th Symposium on Rock Mechanics and the following sections are largely taken from that paper.

Fundamental Concepts

Perhaps the most fundamental concept necessary in the

understanding of residual stress phenomena is that of the self-equilibrating unit. Since residual stresses exist in the absence of loads and of thermal gradients, they must somehow form self-equilibrating units in order to satisfy Newton's second law. Self-equilibrating units that are either macro or micro in nature are possible and residual stresses are sometimes classified as being either macro or microresidual stresses. Examples of both types of residual stresses are discussed in a later section.

A well known result from thermoelasticity is that an increase in temperature results in an increase in volume. If the material is isotropic and homogeneous, a uniform change in temperature will cause a volume change with no accompanying change in the stress field or the shape of the body. On the other hand, temperature gradients induce both changes in volume and in shape. If the change in volume or shape is constrained or would induce a displacement field that is geometrically incompatible, a thermally induced stress field results in order to maintain compatible deformation. The same situation exists regardless of the mechanism that induces the inhomogeneous strain field. This concept is used to explain some of the proposed mechanisms for residual stresses in rock.

The terms residual stress and residual strain are often used interchangably although by definition they are not the same. The term residual strain used in this context refers to the strain field maintained by the residual stress field and should not be confused with the permanent set (or strain) induced by loading a material beyond its yield point and then releasing the load to zero. This permanent set can exist (at least ideally) with no stress while residual strain cannot.

This situation is shown on Fig. 2.

The presence of both residual stress and strain fields leads to the existence of internal residual strain energy. Friedman reports that the internal residual strain energy is commonly found to be of the order of 10^4 ergs/cm^3. These energies are computed using residual strains measured in X-ray diffraction studies or by strain relief methods along with the appropriate modulus of elasticity. As will be shown later, there is preliminary evidence that at least part of the internal residual strain energy in rocks is temperature dependent.

Existence of Residual Stresses and Strains in Rock

Evidence of the existence of residual stresses and strains in rock exists both in the field and from laboratory measurements. In the field, evidence such as the exfoliating of practically unweathered rock which is isolated from active tectonic movements has been reported by Varnes. Further field evidence is supplied by the distortion of saw cuts and drill holes beyond what would normally occur elastically under conditions where the only reasonable explanation is locked in stresses.

Laboratory evidence for the existence of residual stresses and strains has been found using both X-ray methods and strain relief methods. In addition, optical evidence such as undulatory extinction in quartz points toward the existence of residual deformation in crystals.

Mechanisms Producing Residual Stresses in Rock

Several mechanisms producing residual stresses in rocks have been discussed in the references given in this section. These mechanisms are briefly reviewed here for completeness and to point out their relationship to the fundamental

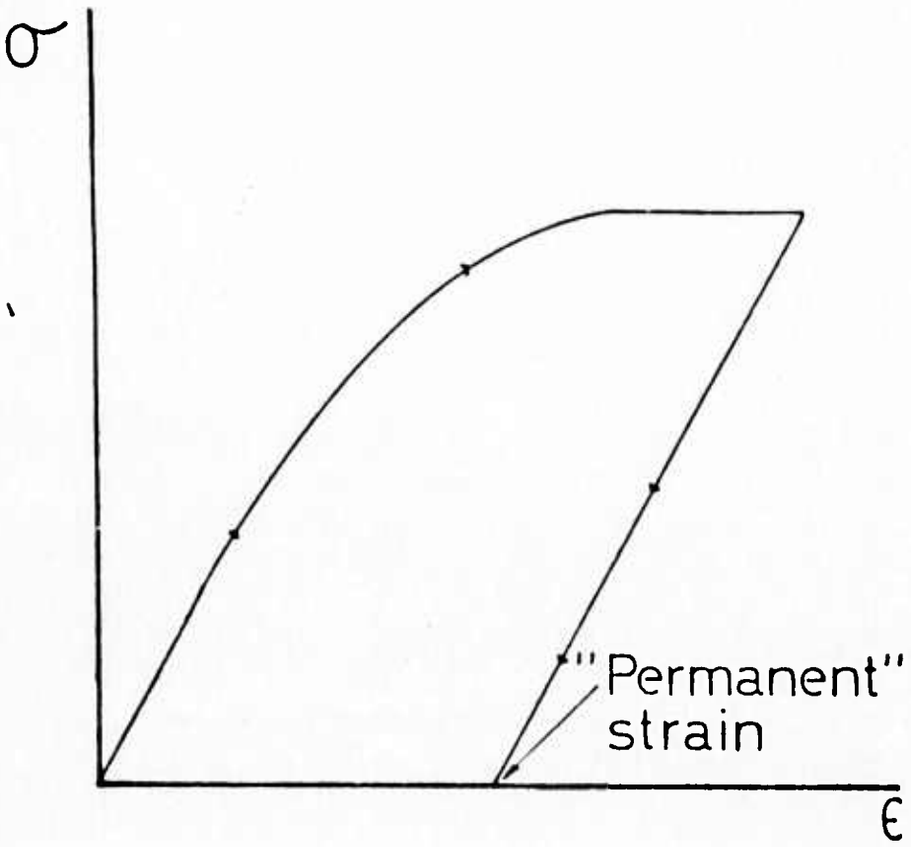

Fig. 2: Stress - strain curve illustrating permanent set.

concepts discussed above. Some variations of previously suggested mechanisms are considered. Most of the mechanisms discussed are micro rather than macro in nature. It should be noted that the designation micro as used here refers to the size of the self-equilibrating unit which may be of the order of several times the average grain size.

The classification of a mechanism as micro may be further subdivided into micro-elastic or micro-dissipative depending on whether elastic elements alone or elastic elements in conjunction with friction elements or viscous elements are used in the model of the mechanism.

Micro-elastic residual stresses develop when a rock containing minerals having different and/or anisotropic coefficients of thermal expansion undergoes a uniform change in temperature. Here the source of nonuniform strain is the nonuniformity of the expansion characteristics coupled with a uniform change in temperature. This mechanism might be referred to as micro-thermoelastic. It should be noted that since the residual stresses and strains in this case vary with temperature the internal residual strain energy will also be temperature dependent. Further, this mechanism suggests that strain relief measurements made on an unconnected piece of rock at depth where the temperature is higher will probably be different than strain relief measurements made on the same piece of rock in the laboratory. Some preliminary evidence pointing to the existence of this mechanism in a medium grained granite is reported in a later section.

Two other examples of micro-elastic residual stresses in rocks are provided by the crystallization of granite under pressure and the cementation of sand grains under high hydrostatic pressure. In both cases, the mechanism is

essentially the same although the scale may be different. Consider the very simple qualitative model shown on Fig. 3. Two springs having different spring constants are compressed by the same amount and are initially independent of each other. If we now connect both springs to the same cross bar and require that the bar can move only parallel to itself, we see that the situation is unchanged as long as the loading condition remains static. However, if the load is removed, both elastic springs attempt to regain their respective initial unstrained positions. This is now impossible because of the newly created bond between the springs and tension will develop in the stiffer element while the more flexible element will remain in compression.

On a smaller scale, the self-balanced stress fields around dislocations in the crystal lattice are examples of elastic residual stresses. Dislocations have been the subject of a considerable amount of research and much information is available. On the smallest scale, microresidual stresses are due to misfitting solute atoms and individual dislocations. c.f. McClintock and Argon (1966)

Chemically induced volume changes can be the source of nonhomogeneous strain that induces residual stresses. This mechanism is sometimes mentioned but to the authors' knowledge has not been discussed in any detail.

Microresidual stresses may also involve dissipative elements such as friction blocks and/or dashpots. As shown in Fig. 4, a self-equilibrating element may consist of a spring and a friction block in a series connected to a spring in parallel. If this unit is loaded beyond the force necessary to slide the friction element and then subsequently unloaded, the spring in series with the friction

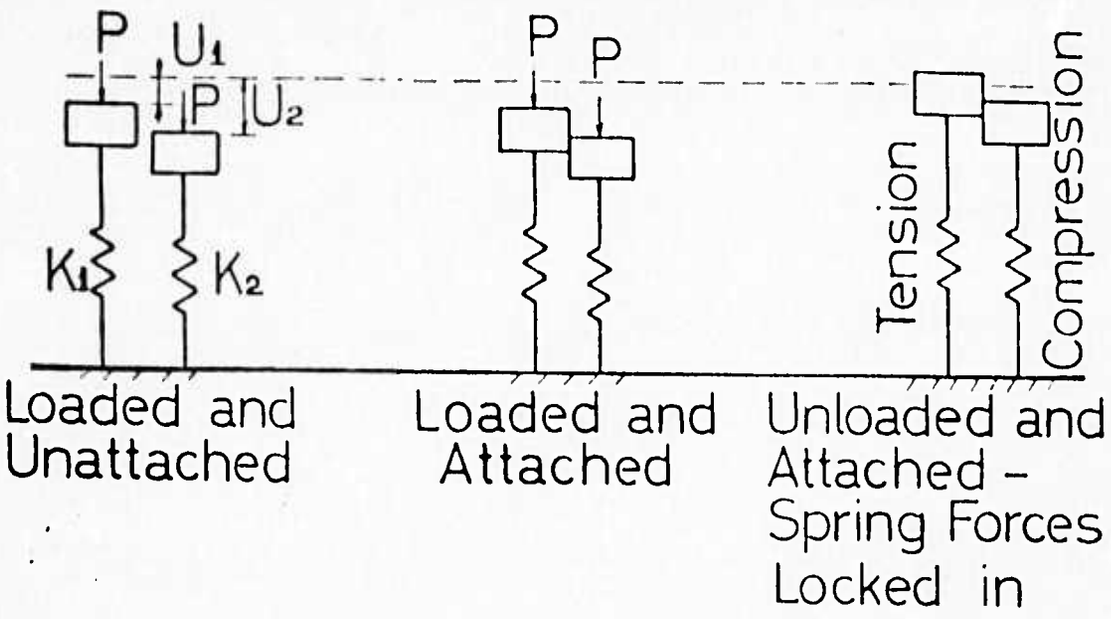

Fig. 3: A purely elastic residual stress mechanism

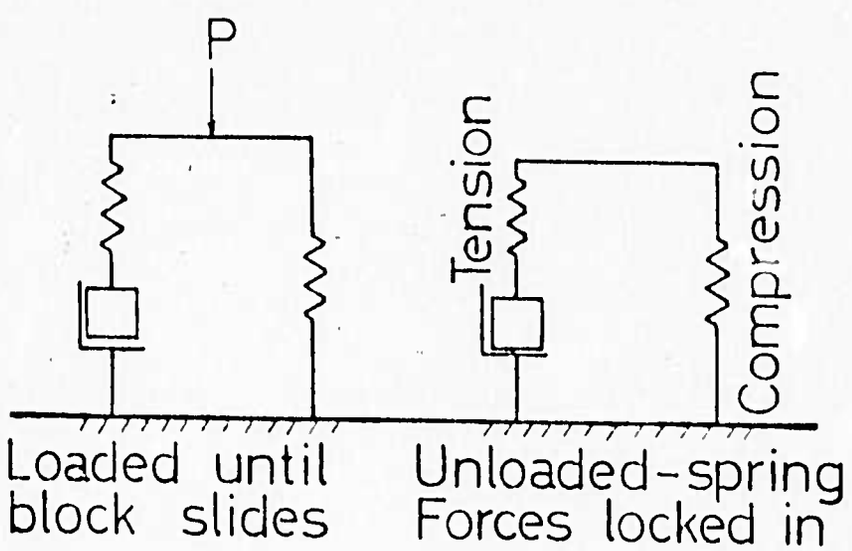

Fig. 4: An elastoplastic residual stress mechanism

element will develop tension while the spring on the other side will remain in compression. In this case, the residual strain field would not be time dependent. On the other hand, if a viscous element has been used rather than a friction element, the resulting strain recovered would be time dependent. Some evidence of time dependent strain relief has been reported by Varnes (1969)and Emery (1964).

On the macro scale, which is taken here to be orders of magnitude greater than grain size, it is difficult to imagine that many of the above discussed mechanisms are operative because of the fragmented nature of much in situ rock. Nevertheless, a macro-dissipative residual stress mechanism usually assumed to operate in ductile metals may be useful in explaining some phenomena. Consider a plate flexed by some external agent to the point that yielding occurs on the upper and lower surfaces to a depth less than half the thickness of the plate. Then an elastic core remains around the neutral surface of the plate. Upon unloading, the elastic core attempts to straighten out and regain its original unflexed position which is now impossible because of the yielding in upper and lower regions of the plate. This situation is shown on Fig. 5.

It should be pointed out that it is likely that more than one of the above mechanisms may be acting simultaneously in any given rock. For example, the thermoelastic mechanism may be acting concurrently with nearly any of the others, or macro induced microresidual stresses are apparently possible. The possible coexistence of several mechanisms complicates the job of attempting to isolate their effects.

Methods for Measuring Residual Strains

Two basic techniques used for measuring residual strains

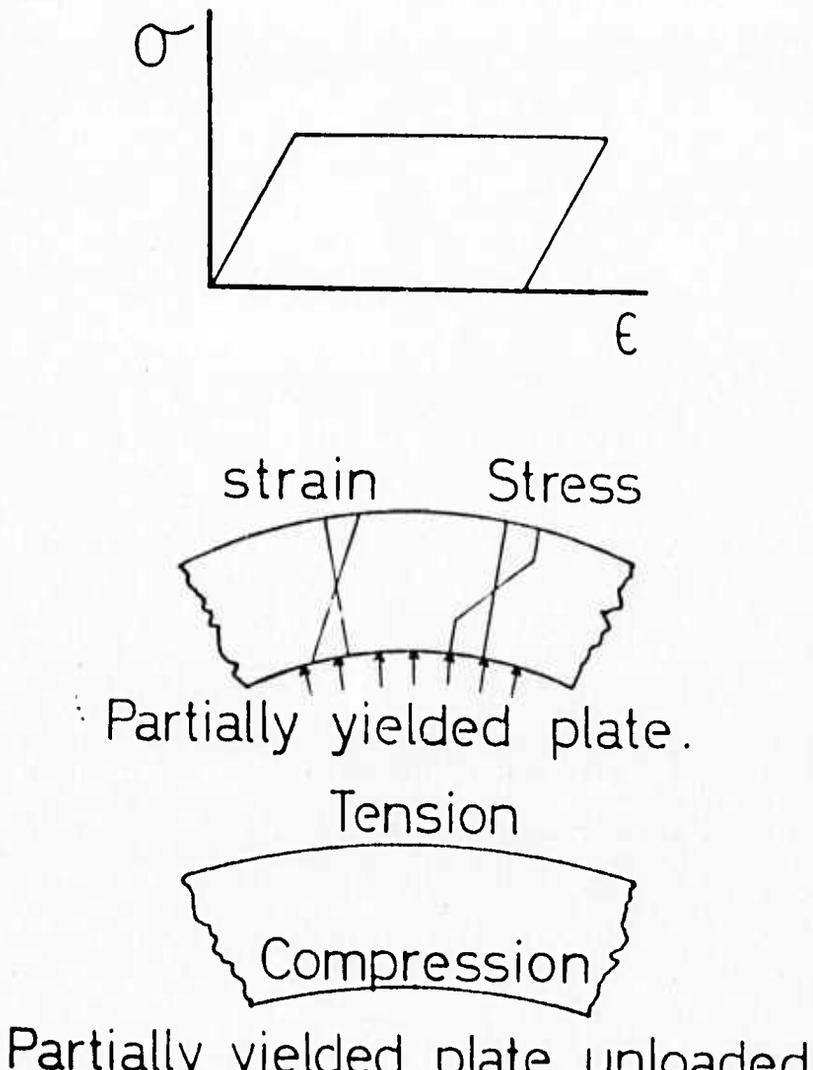

Fig. 5: A macroresidual stress mechanism

are X-ray diffraction and strain relief methods. Measurement of residual strain by X-ray diffraction is discussed by Friedman, (1968) and will not be considered here. The strain relief methods consist of removing some of the rock by sawing, coring, etching or any other means and recording the change in strain in the remaining material. Common techniques include overcoring and undercoring (trepanning) to relive the residual stress field. The amount of strain relieved is usually recorded by bonded electrical resistance strain gages although photoelastic coatings have also been used. The strain changes recorded in the overcoring case may be directly converted to principal stresses and directions provided that the elastic constants for the material are known. It should be noted that compressive stress gives rise to extensional strain relief after overcoring.

The situation is not so straight forward in the undercoring case. Here, resort must be made to elasticity solutions that express the stress field existing before trepanning in terms of the strain relieved.

Both overcoring and undercoring give satisfactory results when used in macrostress situations provided stress gradients are not too high, and are the basis of many in situ stress measurement devices. Unfortunately, there are several difficulties associated with the use of strain relief methods to measure residual strains in relatively small samples of rock or total strains in rock masses where the residual part of the strain relieved is a significant part of the total.

Successive overcoring of the same strain gages shows that strains of the same order are relieved on both the first and the second cuts. Experimental results are reported in a later section for a medium grained granite. If one or more of

the microresidual stress mechanisms are acting, all of the residual strain may not be relieved until the rock is disaggregated down to the grain size. Even then, dislocations may exist in the crystal lattice.

If the strain gage size is of the same order as the average grain size, different results may be expected from different gages with the same orientation depending on whether they are predominately on a grain showing tensile or compressive relief. On the other hand, if the gage size is many times the average grain size, more consistent results should be obtained.

The proximity of the gages to the relief surface may influence the results. This factor is generally accounted for in trepanning but not in overcoring. In a macro field with relatively low strain gradients, there should be no problem. Again the difficulty is associated with measuring microstrain fields. Even in macro fields, difficulty can arise if a plastic zone develops due to the stress concentration around the hole.

If the residual strain field is ideally elastic, there should be no difficulty with time dependent effects. However, time dependent effects have been observed during some preliminary tests run at the South Dakota School of Mines and Technology. Time dependent effects have also been reported by Varnes and Emery (loc. cit.)

Temperature effects previously discussed may also effect the magnitude of residual strains relieved. Further work on temperature effects is planned.

There are difficulties associated with converting strains relieved into stresses. It is likely that the material properties at this scale are anisotropic and vary from grain to grain. Consequently, the use of large scale moduli or an

isotropic modulus may not be valid.

Another potential difficulty with strain relief measurements occurs if a strain gage spans a microcrack in the rock. If the microcrack opens during the relief process, some of the strain recorded by the gage may actually be rigid body movement and not deformation of the material

Further research is required to more definitely establish the effects of the above difficulties. Some recently completed work is reported in following sections.

Laboratory Results

Laboratory tests have been completed on a section of 6 inch core of Redfield granite, 1 5/8 inches thick. This granite has been used in previous studies of residual strain in rock and has been described as

> The granite (Precambrian) from Redfield, South Dakota, is a light reddish brown, medium to coarse-grained rock which consists of major amounts of pink orthoclase feldspar, grey vitreous quartz and minor amounts of black flakes of biotite. In thin section, the rock consists of equigranular, anhedral to subhedral minerals of fine to medium-grained (0.3-3.6 mm) quartz (37%); medium to coarse-grained microcline (51%); coarse-grained (3.6mm) plagioclase (10%); fine-grained (0.5 mm) biotite (2%) and traces of magnetite and apatite. The minerals do not appear to be preferentially oriented; the minerals contain numerous small fractures both at and across grain boundaries.

The section of core used had a smooth surface on all sides.

The sample size and strain gage locations are shown on Fig. 6

The strain gages were initially zeroed and allowed to stabilize under the cooling water. The first cut was made from the back side using a 3 1/4 x 3 3/16 inch bit. This operation overcored the inner six strain gages while simultaneously undercoring the outer five strain gages.

Typical data is shown on Fig. 7 for the rosette formed by the three 1/4 inch single gages, 9,10, and 11. This rosette was overcored by drilling from the back side. The innermost rosette formed by 1/8 inch gages 6,7,and 8 was also overcored by the 3 1/4 inch bit. As shown on Fig. 7, readings were continued after the bit broke through in order to check for possible time dependent effects. Readings were discontinued when two successive readings showed no further significient change in strain.

The initial change in strain, which occured when a 3/16 inch deep kerf was cut on the opposite side of the sample, was greater for the inner rosette. This is contrary to what might be expected. In a macrostress field, with small strain gradients, one would expect that both rosetts should indicate the same magnitude of strain relief. This is taken to be evidence that the residual field in this sample is micro rather than macro in nature.

It is interesting to note that the principal directions indicated by the two rosetts are relatively consistent. For the inner rosette, the principal direction was found to be 135 degrees clockwise from gage 6 while the corresponding direction from the next outer rosette was 143 degrees clockwise from gage 9. Consistency in directions when measuring residual strains by relief methods has previously been reported,

Because of the relatively small amount of strain relieved

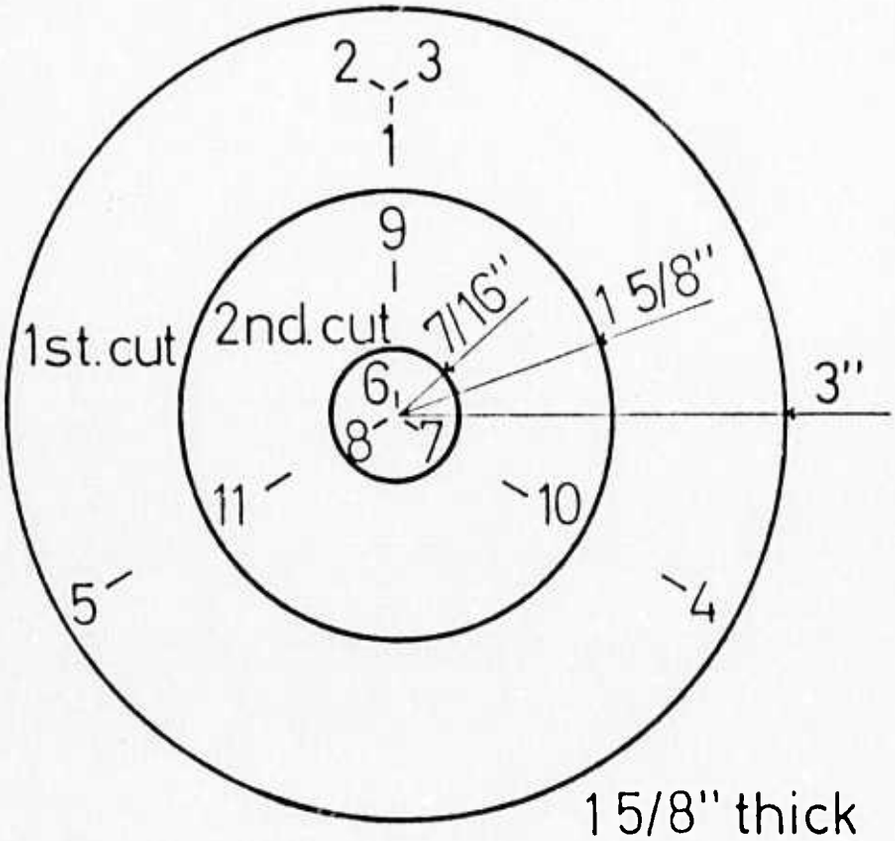

Fig. 6: Typical sample showing location of strain gages.

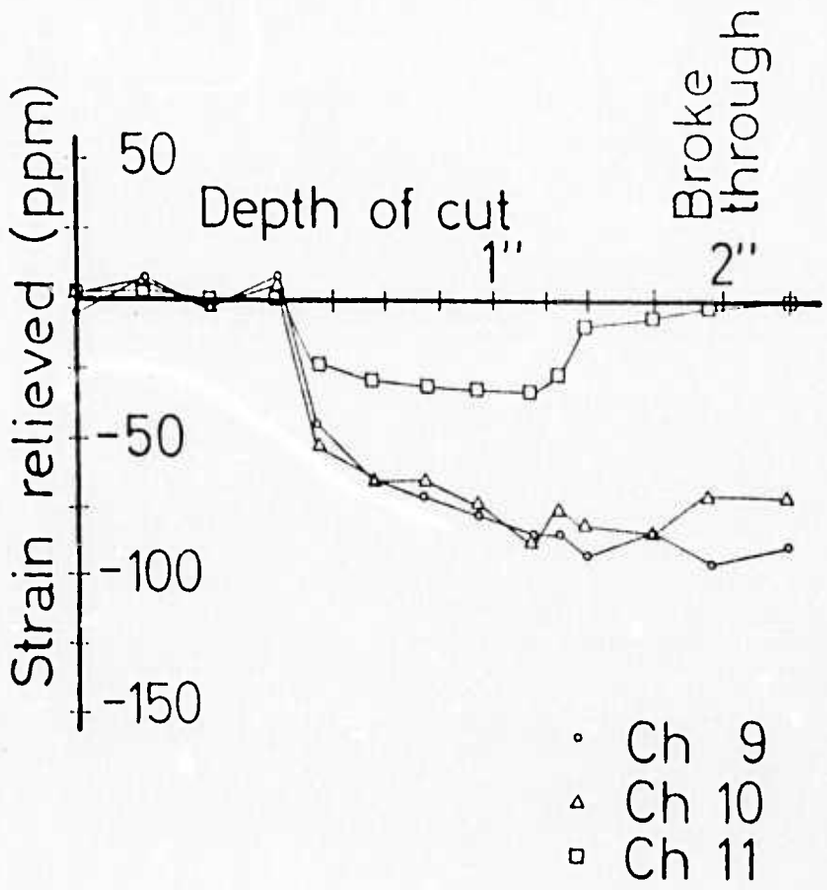

Fig. 7: Strain relieved by cutting from the back with a 3 1/4" bit.

at kerf depths of 11/16, 15/16, and 1 3/16 inches, these readings were averaged to obtain new initial strain readings to compare with strain readings obtained after the bit broke through from the back side. In this case, there appears to be no correlation between either the magnitude of the strain releived or in the principal directions computed from these strains. A comparsion of the results from the two rosettes that were overcored is shown in Table 1.

After the above test had been completed, the same sample was cored again. This time with a 15/16 x 7/8 inch bit from the gage side. Thus the innermost rosette was again overcored while the next outer rosette was undercored. The strain changes registered by gages 6,7 and 8 respectively were-22, -49, and + 6. The principal direction was found to be 46 degrees clockwise from gage 6. Neither the magnitudes nor the principal direction appear to correlate with the overcoring data shown in Table 1.

In both overcoring tests, there were examples of strain gages facing each other across the kerf of the drill bit, e.g., gages 6 and 9 in the second test. One pair of these gages in each test registered changes in strain with opposite signs indicating extension on one side and contraction on the other side of the kerf. This is taken as further evidence of the micro nature of the residual strain field in this piece of granite. A macroresidual strain field would have registered consistent extension or contraction on both sides of the kerf provided that strain gradients were relatively small.

To further confirm the micro nature of the residual strain field and the influence of gage size relative to grain size, a temperature dependent test was devised. This test was conducted on the 7/8 inch core and the annular shell remaining from the second overcoring and still having strain

Depth of Cut	3/16"						1 5/8"=sample thickness					
	Innermost Rosette			Next Outer Rosette			Innermost Rosette			Next Outer Rosette		
Channel	6	7	8	9	10	11	6	7	8	9	10	11
Strain Change (ppm)	-73	-67	-79	-47	-54	-25	11	33	5	-9	-1	27
Principal Direction (degrees)	135°			143°			126°			67°		
Notes	Relatively good agreement in principal directions						New initial strains taken to be average of strains at depths 11/16, 15/16, and 1 3/16					

Table 1: Comparison of results from simultaneously overcoring two strain gage rosettes.

gages 6 through 11 intact. The inner rosette and two of the gages on the outer shell were treated as live gages while the remaining gage on the outer shell served as the temperature compensating gage. Initial readings were taken until they were stable at room temperature. The two samples of granite were then placed in a freezer at zero degrees Fahrenheit. Fig. 8 shows the change in strain on the three active gages making up the inner rosette when gage 10 was used as the common temperature compensation gage. The same test was run with gage number 11 on the outer ring acting as the compensating gage.

As shown on Fig. 8, temperature compensation was not effective throughout the duration of the test. The immediate drop in strain that occured when the samples were placed in the freezer was probably due to surface cooling and the fact that the amount of surface area per unit volume was different for the 7/8 inch core and the outer shell containing the compensating gage. However, if temperature compensation were effective, after a period of time, the gages should have again registered no strain. The strain change-time curve shown on Fig. 8 indicates that after 80 minutes at zero degrees, the gages registered significant strains showing extension at gages 6 and 8 and contraction at gage 7.

Results from the other temperature test when gage 11 was used as the compensating gage were similar to those shown on Fig. 8 except that the magnitudes of the strains relieved were 315, 241, and 313 ppm respectively for gages 6, 7 and 8 after approximately 95 minutes at zero degrees. The principal directions computed from the strain changes were 26 degrees for the case shown on Fig. 8 and 30 degrees for the other case. Again the magnitudes of the strain changes do not correlate but their principal directions agree reasonably well.

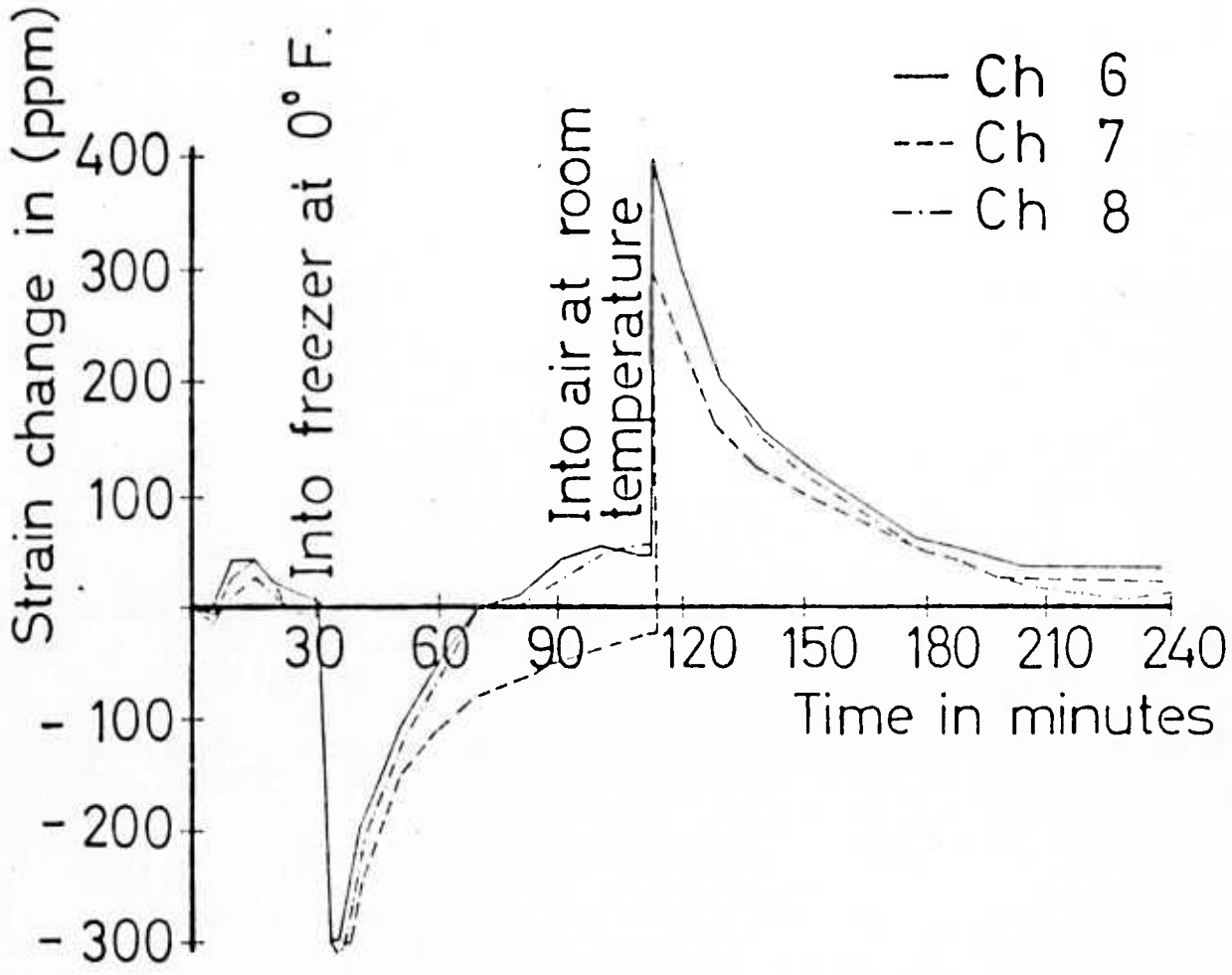

Fig. 8: Strain change verses time resulting from temperature change.

These results may be interpreted as follows: the large difference in strain magnitudes between the two tests is probably due to the fact that the strain gages used for temperature compensation did not span a representative distribution of the minerals making up the rock, i.e., the gage length was too small in comparsion to the mean grain size. In one case the grains under the compensating gage had a markedly different effective coefficient of thermal expansion than in the other. If the only difference between the two tests were the coefficient of thermal expansion of the material under the compensating gage, all of the live gages should have registered the same change in strain. Since this was not the case, it seems likely that the residual strain field is temperature dependent in this sample. This position is supported by the relatively good agreement in the principal directions computed from the test data.

Qualitative System Models

The models shown of residual stress mechanisms are readily understood when they are considered one at a time as previously discussed. However, in the actual case it appears likely that two or more of the mechanisms act simultaneously. Furthermore, a large number of self-equilibrating mechanisms interact with one another. The behavior of such complex systems is rather difficult to visualize. As a consequence, Varnes has fabricated and tested physical models to aid in understanding residual stress phenomena. These models consist of elastic, plastic, and viscous elements and are described in Varnes (1969).

As an alternative to physical models, numerical models can be used. Numerical models have the advantage of being easily adapted to new configurations as they are encountered. Also, parameter studies can be made to determine the sensitivity of the behavior to changes in relative stiffness, anisotropy, viscosity, etc.

A residual stress modeling digital computer program is presently being developed at the South Dakota School of Mines and Technology. The first step has been to develop a finite element program that employs self-equilibrating elements. An example of such an element is shown on Fig. 9. The element is composed of eight separate elastic springs connected at five nodal points. The interior nodal point may be eliminated by a substructure analysis leaving only the four corner nodes. Each corner node has two degrees of freedom. This basic square or rectangular rock sample. An example is shown on Fig. 9.

Each element in the rectangular array of elements (the model) shown on Fig. 9 is connected to its adjoining elements only at the corner nodal points. Residual stresses are induced into the elements by allowing the inner springs in each element to have a different coefficient of thermal expansion than the springs forming the outer square. The temperature of the model is then changed uniformly. If the inner springs have a higher coefficient of thermal expansion and if the temperature change is an increase, the inner springs in each element will develop compression and the outer springs tension. The model at this stage contains residual stresses.

A cut in an outer spring of an element in the model may be simulated by reducing the stiffness of that particular spring. It should be noted that reducing the stiffness

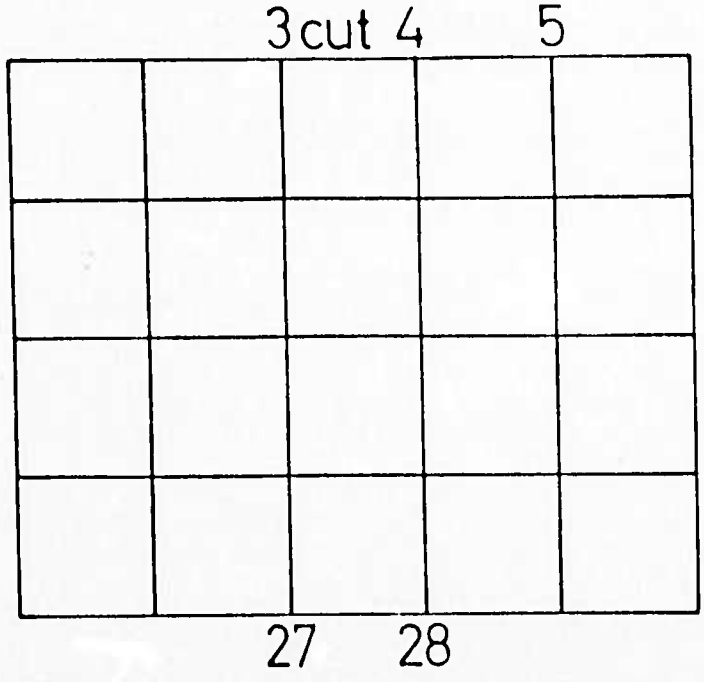

Elastic finite element model

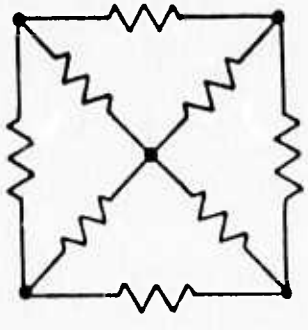

Typical self-equilibrating element

Fig. 9: A simple finite element model for residual stress phenomena

of a particular spring in one of the outer elements results in a change in displacement of all of the nodes in the model.

Some preliminary results obtained from the finite element model are shown on Fig.10 where the change in length of two typical springs from the model are plotted versus the percent reduction in stiffness of the outer horizontal spring connecting nodes 3 and 4 in element number 3. The parameter "c" equals the ratio of the stiffness of the inner springs in an element to the stiffness of the outer springs in the element. All elements are identical prior to the reduction in stiffness of the spring connecting nodes 3 and 4. The interior coefficients of thermal expansion are 1.414 times the outer coefficients.

The results shown on Fig.10 illustrate the importance of the stiffness ratio c to the response of the system to the reduction in stiffness of one outer spring. Cutting the outer spring between 3 and 4 results in an extentional change in length on both the top and bottom surfaces of the model when c = 4 and a contractional change when c = 0.25 up to the point where the cut has reduced the stiffness by 75%. At this point, the spring connecting nodes 4 and 5 had been dominated by lateral contraction, after this point, vertical movement causing extension begins to play an important role in the change in length of the spring. The single most impressive feature of the results shown on Fig.10 is the complexity in the response of such a simple model. It should be noted that the change in strain resulting from the first cut on the back side of the granite sample discussed in the last section might be explained by a numerical model similar to the one discussed here.

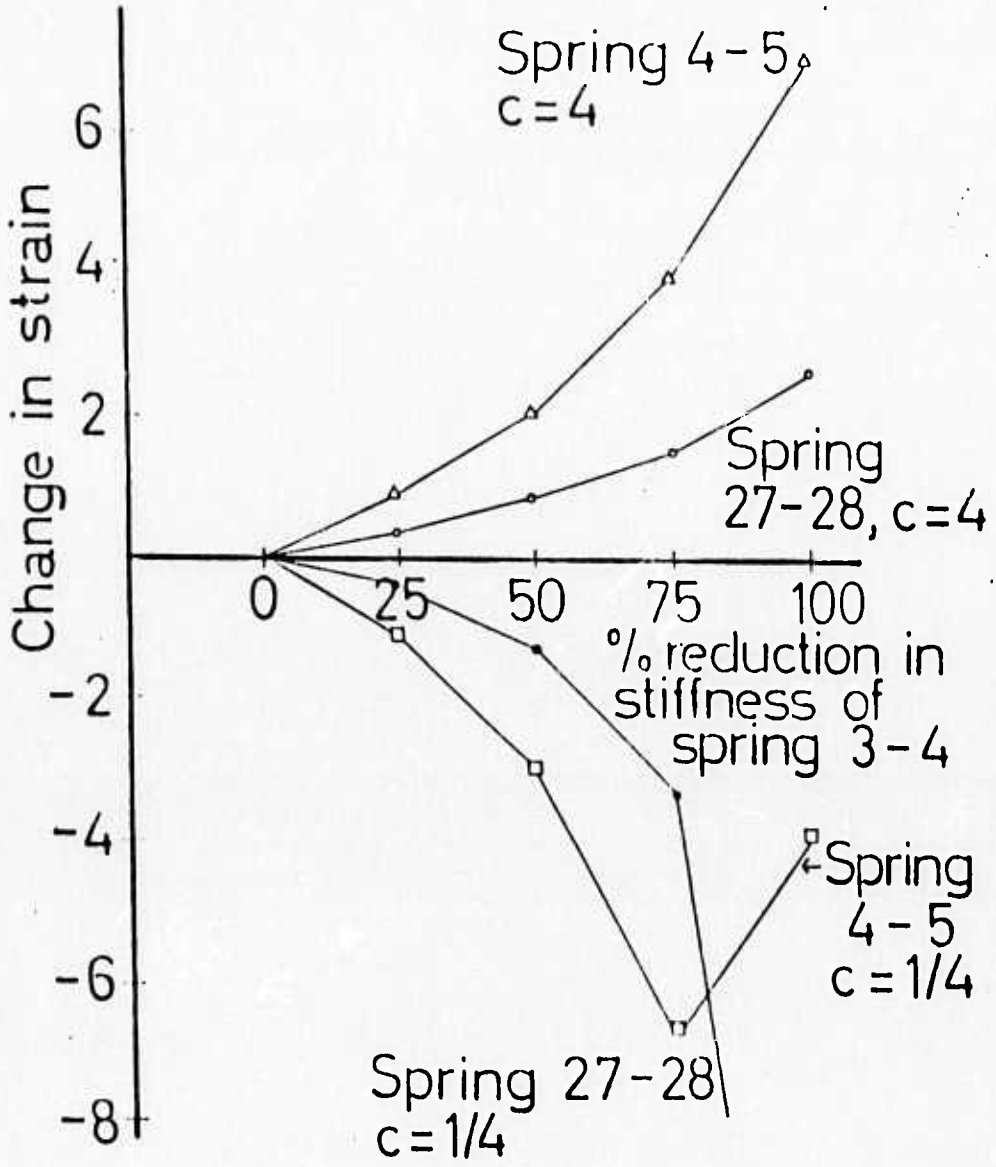

Fig. 10: Results from numerical model.

It is easy to imagine more complex models. For example, the simple square element could be replaced by a self-equilibrating hexagon or octagon with interior springs radiating from a single interior nodal point and each having its own chacteristics. Friction elements and/or vicous elements could be added in series and/or parallel to the spring elements. A whole realm of mixed element models could be developed having different shapes and chacteristics to attempt to better simulate the behavior of actual rocks. All of the suggested models could be extended to three dimensions. Practically speaking, storage space in the computer soon becomes a problem and limits extent of the simulation.

At this stage of development, the primary value of both physical and numerical models appears to be their use as an aid in understanding the complex behavior of large systems containing self-equilibrating elements. Presently, it is not feasible to obtain quantitative information from these models, hence they are referred to as qualitative models.

Discussion

Results from both laboratory tests and a very simple mathematical model indicate that the response of arrays of interconnected self-equilibrating units is complex and not easily visualized. The laboratory test results seem to indicate that at least part of the residual strain field is temperature dependent and the size of the strain gage relative to the grain size is probably an important parameter.

The likely existence of a temperature dependent residual strain field suggests that thermal weakening of some rocks may be due to residual stresses changing with temperature. It is anticipated that a set of controlled

experiments will be devised to investigate this hypothesis.

The fact that both the laboratory results and the numerical model indicate that strains may be registered on the opposite side of a sample from where a cut is made. It appears likely that there may be a shape effect, i.e., the size and shape of the sample probably influence the amount and distribution of the strain relieved.

Future work on residual stresses in rock will entail studies of the gage size to grain size ratio as well as the grain size to sample size ratio. More tests will be run to attempt to define temperature dependence of the residual strain fields in rock. Strains relieved at different positions on the surface of a sample due to a hole cut at one point should be measured. Numerical modeling will continue to help in the understanding of residual stresses in rock.

V Data Reduction

Reduction of measured strain data from the deep hole device to in situ stresses can be accomplished in any of several ways. A combination analytical - experimental technique was described in the final report of the first year's work on this project and also in a paper by Hoskins and Oshier published in the 14th Symposium on Rock Mechanics. This method is summarized in the section entitled Experimental Method.

Sateesha working on this project developed a three-dimensional finite-element code for reduction of data from the deep hole device. Portions of his thesis are summarized in the section entitled Numerical Method.

Russell also working on this project produced an approximate analytical solution for data reduction. His work was presented at the 15th Symposium on Rock Mechanics

and is summarized in the section entitled Analytical Method.

Experimental Method

Hiramatsu and Oka (1962) have given the components of stress in an elastic infinite body surrounding a cylindrical borehole as follows:

$$\sigma_r = \alpha_1\left(1-\frac{a^2}{r^2}\right) + \alpha_2\left(1-4\frac{a^2}{r^2}+3\frac{a^4}{r^4}\right)\cos 2\theta + \alpha_3\left(1-4\frac{a^2}{r^2}+3\frac{a^4}{r^4}\right)\sin 2\theta$$

$$\sigma_\theta = \alpha_1\left(1+\frac{a^2}{r^2}\right) + \alpha_2\left(-1-3\frac{a^4}{r^4}\right)\cos 2\theta + \alpha_3\left(-1-3\frac{a^4}{r^4}\right)\sin 2\theta$$

$$\sigma_\zeta = \gamma_1 - \frac{2\lambda}{\lambda+\mu}\,\alpha_2\frac{a^2}{r^2}\cos 2\theta - \frac{2\lambda}{\lambda+\mu}\,\alpha_3\frac{a^2}{r^2}\sin 2\theta$$

$$\tau_{\theta\zeta} = \gamma_1\left(1+\frac{a^2}{r^2}\right)\cos 2\theta + \gamma_2\left(1+\frac{a^2}{r^2}\right)\sin\theta$$

$$\tau_{\zeta r} = \gamma_1\left(1\,\frac{a^2}{r^2}\right)\sin\theta - \gamma_2\left(1\,\frac{a^2}{r^2}\right)\cos\theta$$

$$\tau_{r\theta} = \alpha_2\left(-1-2\frac{a^2}{r^2}+3\frac{a^4}{r^4}\right)\sin 2\theta + \alpha_3\left(1+2\frac{a^2}{r^2}-3\frac{a^4}{r^4}\right)\cos 2\theta$$

In the sidewalls of a borehole subjected to a fluid pressure P

$$\sigma_r = P$$

$$\sigma_\theta = 2\alpha_1 - 4\alpha_2\cos 2\theta - 4\alpha_3\sin 2\theta + P$$

$$\sigma_\zeta = \beta_1 - \frac{\alpha_2}{\nu}\cos 2\theta - \frac{\alpha_3}{\nu}\sin 2\theta + P$$

$$\tau_{\theta\zeta} = 2\gamma_1\cos\theta + 2\gamma_2\sin\theta$$

$$\tau_{\zeta r} = 0$$

$$\tau_{r\theta} = 0$$

When r, θ and ζ are the axes of a cylindrical coordinate system, ν = (Poisson's ratio) $= (\lambda+\mu)/2\lambda$, and the α's β's and γ's are combinations of direction cosines.

The stress strain relations can be written

$$\epsilon_\theta E = \sigma_\theta - \nu(\sigma_r + \sigma_\zeta)$$

$$\epsilon_\zeta E = \sigma_\zeta - \nu(\sigma_r + \sigma_\theta)$$

$$\gamma_{\zeta\theta} G = \tau_{\zeta\theta}$$

Now from the three strain gage rosettes in the device we shall determine ϵ_θ, ϵ_ζ, and $\gamma_{\zeta\theta}$ each at ϕ, $\phi+120°$ and $\phi+240°$ in the borehole walls. We thus have 9 equations with which to calculate the 3 principal stresses P_1, P_2, and P_3 and their directions of action relative to the borehole axis and an arbitrarily selected direction. This much of the analysis is similar to Leeman and Hayes (1966). The trepanning technique does not accomplish complete stress relief, however. The percentage of stress relief achieved depends upon the dimensions of the strain gages and the trepanning hole and theposition of the gages relative to the hole. In addition the friction bonded strain gages may not be 100% efficient at responding to changes in strain. These two factors can be combined and experimentally determined to yield an overall value for the efficiency of this measurement device.

The efficiency of friction bonded strain gages themselves is a function of their design and the normal stress used to hold them in contact with the borehole walls. Laboratory tests so far show that 85% is a typical figure for the efficiency of the gages that we have made. We plan initially at least to individually calibrate each

rosette of friction strain gages before using them in the deep hole device.

Numerical Method

General

The Finite-Element Method, now widely accepted in engineering mechanics, is particularly well suited for the solution of boundary value problems of a geological nature. It can be easily adapted to the solution of systems characterized by inelastic, anisotropic, heterogeneous material properties, of any exterior configurations containing structural discontinuities, and subjected to any statically viable boundary conditions of load or displacement. The main advantages of the finite-element method, as compared to other numerical techniques, such as the classical finite difference formulation, have been described by Zienkiewicz (1971), Clough (1965), and Felippa and Clough (1970). Exclusive emphasis in this chapter will therefore concern the applications of finite-element methods for solving geological problems, and an important practical problem. for which a closed form solution is available, will be presented to illustrate the method.

The range of specific problems encountered in geology is large, but some typical examples that have been fully worked out utilizing the finite-element method include (I) behavior of rocks under static and dynamic loads, (II) seismic response and propagation of stress waves, (III) heat conduction, (IV) fluid flow in porous media, and (V) distribution of magnetic and graviational potential. Many of the fundamental problems in structural geology, geophysics, geohydrology, geomorphology, glacialogy, and engineering geology can be included in the above categories.

Very few authors have attempted to solve geological

problems applying the principles of classical mathematical physics. Hafner (1951) used the Airy stress function of classical elasticity to obtain two-dimensional solutions for stress distributions caused by several arbitrarily defined forms of boundary forces, and constructed the potential fault surfaces based on the original stress distribution. Sanford (1959) used an approach similar to that of Hafner for the theoretical analysis of fault structures. A Fourier series approximation was used to define the displacement boundary condition at the base of a homogeneous elastic layer. Howard (1966) applied Sanford's theory for the analysis of William Range Thrust Fault in Middle Park, Colorado.

The stress function solutions thus obtained from highly idealized models have proven to be both stimulating and valuable. However, with few exceptions modification of stress function solutions to better fit given field situations has rarely been attempted. Even with the available solutions, the restrictive assumptions involved are often ignored. To start with, our conception of the real problem is in itself a model. In geologic problems isotropic elasticity cannot always be assumed, body forces must be taken into account and the lateral and vertical variation in material properties that is generally present must be considered. Well-defined discontinuities may be present and progressive failure of some kind may be induced by the assumed boundary force and displacement conditions. The situation gets more complicated if the mechanism is path dependent, i.e., if the final state of stress, strain or displacement depends upon the manner in which the surface tractions, displacements and body forces obtain their final values.

The effect of the complexities cited above cannot be adequately determined without recourse to analytical and experimental evaluation. Existing closed-form mathematical tools may be suitable for solution of only a few such problems, depending on the nature of the parameter (e.g. some classes of anisotropy). In each of the above situations, the finite-element method is sufficiently versatile for definite evaluation of the problem.

To geologists, the finite-element method has thus opened up the possible exploration of stress distributions in a large variety of complex situations of geologic importance. Such distributions are important not only for problems of faulting but also for folding and ductile deformation in general. Dietrich and Carter (1968) have used the finite-element method to study the stress history of folding.

The deformation of rock associated with cylindrical underground excavation has been investigated by several authors. With few exceptions the problem has been treated as a two-dimensional case and one of the principal stress directions is frequently assumed to coincide with the axis of the borehole. The orientation of the principal stresses underground is, in general, not known and it must be assumed that the axis of a borehole does not coincide with a principal stress direction. Such a general situation can only be analyzed by a three-dimensional analysis and this provides an excellent testing ground to check the validity of three-dimensional finite-element analysis.

THREE-DIMENSIONAL FINITE-ELEMENT STRESS ANALYSIS COMPUTER MODEL STUDIES

The finite-element technique used in this study is based on the displacement or stiffness method of analysis first developed by structural engineers for aircraft industry. These programs are capable of analyzing any three-dimensional structure subjected to any general type of loading. However, the applied stress field is unknown in the borehole-trepanning hole intersection problem under consideration and paradoxically, knowing the stress field acting on the model is tantamount to determining the primary stress field. To circumvent this difficulty, the method of strain coefficients is adopted and is described in the following paragraphs.

The method of strain coefficients has been used by Clough to solve a two-dimensional tunnel problem where the cross section was not circular. For the borehole-trepanning hole intersection problem, the following can be considered a general three-dimensional algorithm for determining the primary stresses from strain measurements on the sidewalls of a borehole.

1. Choose a three-dimensional finite-element model

consisting of a vertical borehole in the middle as shown in Figure 11 The model consists of a finite number of elements interconnected at corners or nodal points. This physical idealization of a solid as an assemblage of finite-elements involves no mathematical approximation. The only approximation is in assuming a displacement function for each element. The usual procedure is to use a linear displacement function. The finite-element solution can be shown to converge to the exact solution as element size is reduced to a point.

2. Apply six unit stress fields (σ_x σ_y σ_z τ_{xy} τ_{yz} τ_{zx}) separately on the model without trepanning holes and determine the strains at gage points from a three-dimensional finite-element analysis. Let these strains (Figure 12 be

$\varepsilon_{b1}^{(i)}$ $\varepsilon_{b2}^{(i)}$ $\varepsilon_{b3}^{(i)}$ at position (1) - $\theta=\pi/2$ (fig. 3.1),

$\varepsilon_{b4}^{(i)}$ $\varepsilon_{b5}^{(i)}$ $\varepsilon_{b6}^{(i)}$ at position (2) - $\theta=7\pi/6$ (fig. 3.1),

and $\varepsilon_{b7}^{(i)}$ $\varepsilon_{b8}^{(i)}$ $\varepsilon_{b9}^{(i)}$ at position (3) - $\theta=11\pi/6$ (fig. 3.1),

$i=1,2,\ldots\ldots,6$, where the first subscript 'b' indicates strain in the model before trepanning and the second subscript gives the gage location. The superscript (i) represents the applied stress field. Thus i=1 corresponds to σ_x, i=2 corresponds to σ_y etc.

3. Now consider the model with three trepanning holes 120^o apart on the sidewalls of the borehole. Again apply

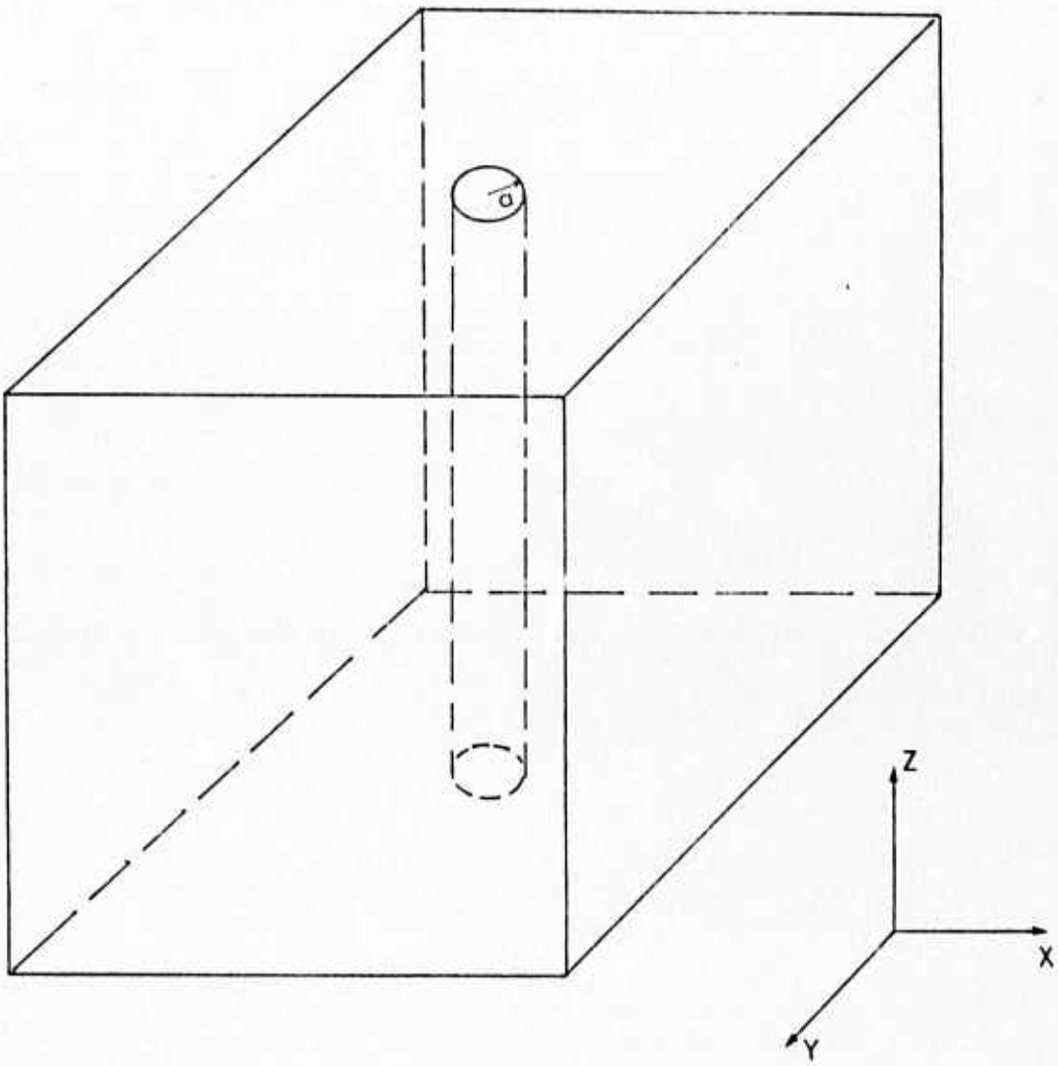

Fig. 11 Three-dimensional finite element model

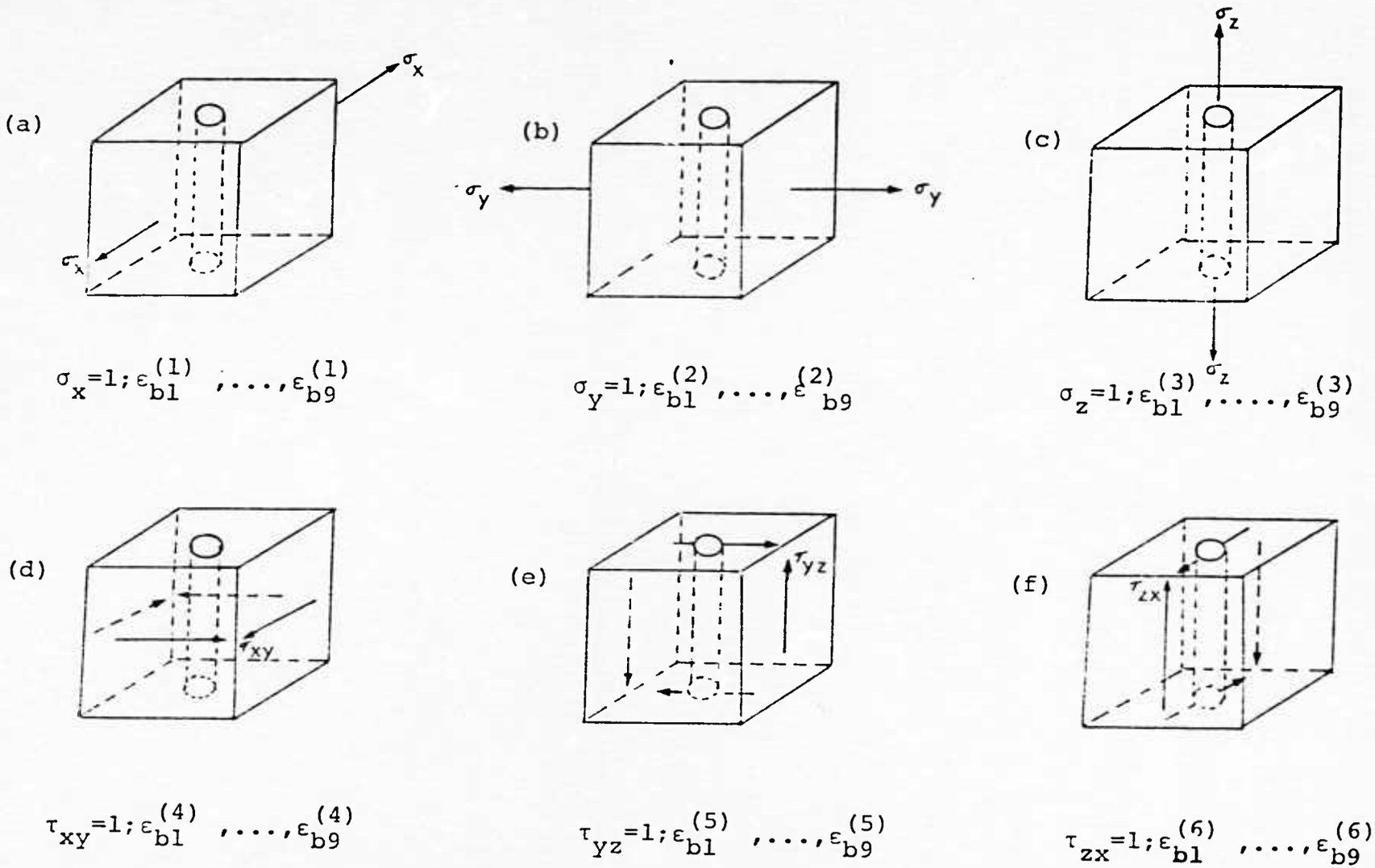

Fig. 12 Applied unit stresses and asscciated strains at gage points for the model without holes

six unit stress fields (σ_x σ_y σ_z τ_{xy} τ_{yz} τ_{zx}) separately and determine the strains at the gage points from a three-dimensional finite-element analysis. Let these strains (Figure 13) be

$\varepsilon_{t1}^{(i)}$ $\varepsilon_{t2}^{(i)}$ $\varepsilon_{t3}^{(i)}$ at position (1) - $\theta=\pi/2$,

$\varepsilon_{t4}^{(i)}$ $\varepsilon_{t5}^{(i)}$ $\varepsilon_{t6}^{(i)}$ at position (2) - $\theta=7\pi/6$,

and $\varepsilon_{t7}^{(i)}$ $\varepsilon_{t8}^{(i)}$ $\varepsilon_{t9}^{(i)}$ at position (3) - $\theta=11\pi/6$,

$i=1,2,.....,6$, where the first subscript 't' indicates strain in the model with trepanning holes.

4. Compute the resulting relaxation strains or strain coefficients by subtracting strains obtained in step 3 from the corresponding strains determined in step 2. Thus

$$\varepsilon_{rj}^{(i)} = \varepsilon_{bj}^{(i)} - \varepsilon_{tj}^{(i)}; \quad j=1,2,.....,9; \quad i=1,2,.....6,$$

where the subscript 'r' indicates the relaxation strain.

5. Let the measured value of relaxation strains in a three-dimensional stress field be denoted by

ε_{m1} ε_{m2} ε_{m3} at position (1) - $\theta=\pi/2$,

ε_{m4} ε_{m5} ε_{m6} at position (2) - $\theta=7\pi/6$,

and ε_{m7} ε_{m8} ε_{m9} at position (3) - $\theta=11\pi/6$,

where the first subscript 'm' indicates the measured strains and the second subscript gives the gage location.

Let us assume that the strain relieved at any of the three θ positions does not affect the measured strains at the remaining two positions. This assumption is valid

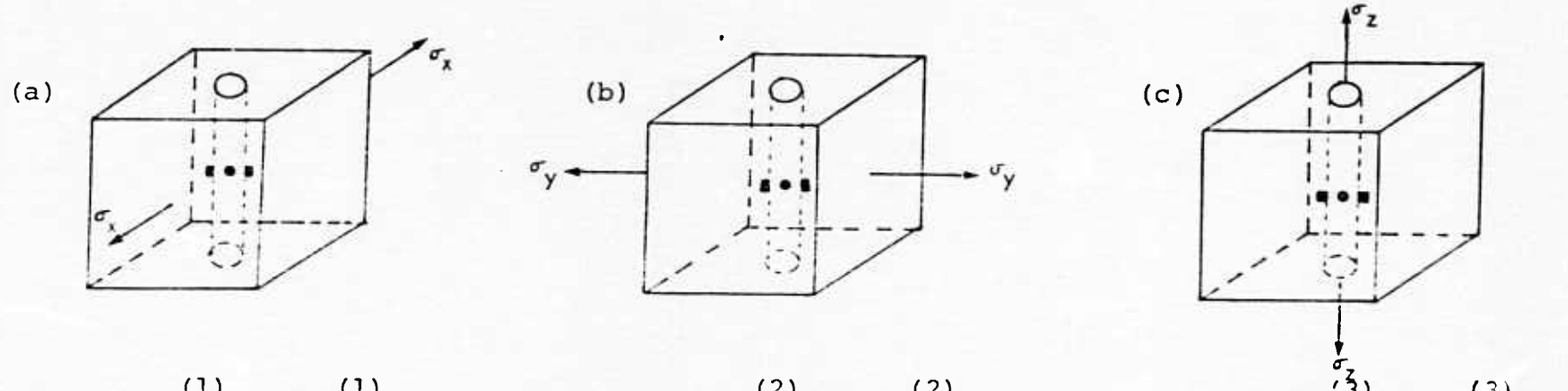

$\sigma_x=1;\ \varepsilon_{t1}^{(1)},\ldots,\varepsilon_{t9}^{(1)}$ $\sigma_y=1;\ \varepsilon_{t1}^{(2)},\ldots,\varepsilon_{t9}^{(2)}$ $\sigma_z=1;\ \varepsilon_{t1}^{(3)},\ldots,\varepsilon_{t9}^{(3)}$

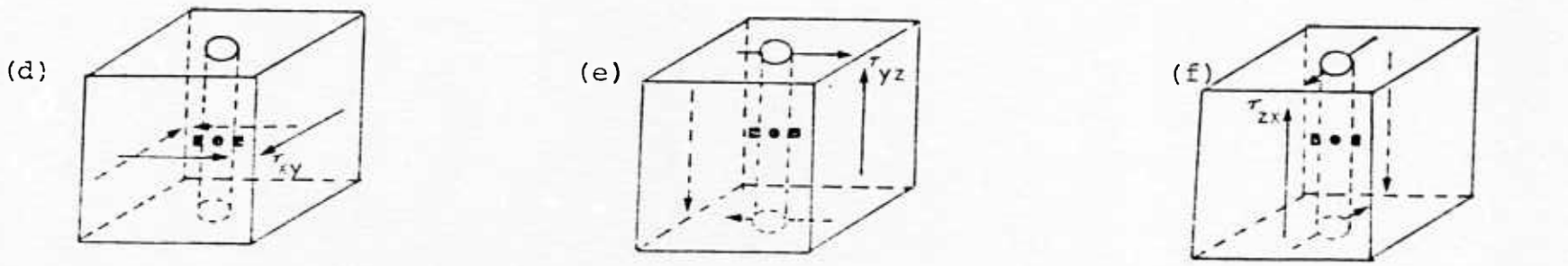

$\tau_{xy}=1;\ \varepsilon_{t1}^{(4)},\ldots,\varepsilon_{t9}^{(4)}$ $\tau_{yz}=1;\ \varepsilon_{t1}^{(5)},\ldots,\varepsilon_{t9}^{(5)}$ $\tau_{zx}=1;\ \varepsilon_{t1}^{(6)},\ldots,\varepsilon_{t9}^{(6)}$

Fig. 13 Applied unit stresses and associated strains at gage points for the model with three trepanning holes

since the trepanning hole diameter is very small in comparison with borehole diameter and the spacing between any two holes is several times the hole diameter along the borehole circumference. Let us further assume that the model material behaves in a linearly elastic manner and the principle of superposition is valid. The relationship between the measured strain and the unknown stress components can now be written by summing the products of the stress components and the associated strain coefficients for each gage location. Therefore

$$\varepsilon_{rj}^{(1)}\sigma_x + \varepsilon_{rj}^{(2)}\sigma_y + \varepsilon_{rj}^{(3)}\sigma_z + \varepsilon_{rj}^{(4)}\tau_{xy} + \varepsilon_{rj}^{(5)}\tau_{yz} + \varepsilon_{rj}^{(6)}\tau_{zx} = \varepsilon_{mj},\ j=1,2,.....9 \qquad (3.24)$$

or $$(\varepsilon_r)\{\sigma\} = \{\varepsilon_m\} \qquad (3.24a)$$

Since there are nine equations and only six unknowns, the system is overdetermined and the additional measurements are said to be overcomplete. Such cases are very common in practice since we measure more quantities than there are unknowns, to avoid the influence of statistical fluctuations. The problem can be solved by two different approaches. In the first, six independent equations are arbitrarily chosen and solved for the six unknown stress components. All possible combinations of six equations that do not result in a singular system are then solved. The solution vectors so obtained are then used for comparison and cross checking. Using equations (3.19) and (3.20), it can be shown that only 18 combinations are

are possible. Many of these combinations may result in ill-conditioned system of equations. In the second approach, which is more rational, we solve the problem by means of the maximum likelihood method from the theory of adjustments. The best estimates for the unknown stress components are obtained by applying the method of least squares. The normal equations are obtained as

$$(\varepsilon_r)^T \cdot (W) \cdot (\varepsilon_r) \cdot \{\sigma\} = (\varepsilon_r)^T \cdot (W) \cdot \{\sigma_m\} \qquad (3.24b)$$

where (W) = weight matrix, and the superscript T designates the transpose of a matrix.

6. Compute the principal stresses $\sigma_{(1)}$, $\sigma_{(2)}$ and $\sigma_{(3)}$, and their orientations from the six stress components obtained in step 5.

The primary stresses in the rock are now completely determined.

Several computer programs were developed to carry out the analysis described in the above steps. These programs are completely compatible with one another and a description of their use is given in the Appendix.

A large scale, high-speed digital computer is required, owing to the large number of elements normally required to adequately model the borehole-trepanning hole intersection. A CDC-3400 computer with 32K word storage was used in this study.

SUBSTRUCTURE METHOD OF ANALYSIS

The number of finite-elements required to obtain the

stress distribution at the borehole-trepanning hole intersection is so large that the available computer facilities cannot conveniently accomodate the problem. To overcome this difficulty, the SUBSTRUCTURE METHOD of analysis is employed.

The substructure method of analysis is well known to structural engineers and is usually applied to such large structures as aircraft frames, multi-story buildings and ships. Each of these can be considered to consist of a number of substructures obtained from structural partitioning. Even though the partitioning can be arbitrary, it is preferable to make structural partitioning correspond to physical partitioning. An aircraft frame, for example, might be considered to consist of wing, tail and fuselage components.

The fundamental principles of substructure analysis have been clearly outlined by several authors, for example Przemieniecki 1968 using a displacement approach and Argyris 1955 / using redundant interaction force concepts. The most compact treatment, and that most generally suitable for programming is the displacement method and this is used in the following condensed theory.

In the substructure method, the substructures are treated as if they were complicated finite-elements, interconnected at terminal nodes to form the overall structure. In the problem under consideration, the finite-element containing the trepanning hole is treated as a substructure.

The stiffness matrix of the substructure is determined by subdividing the substructure into a number of smaller, simple, finite-elements, computing the simple element stiffnesses and assembling the global stiffness matrix of the substructure, and condensing the substructure stiffness to eliminate the internal degrees of freedom. The resulting substructure stiffness is used to develop the overall stiffness matrix of the present structure which is analyzed for any applied external loading. The detailed solutions for the substructure are obtained by determining the internal node displacements and then substituting the displacement values in the expressions for substructure stresses and strains.

In carrying out the above analysis, the continuity of displacements is violated at the substructure-parent structure boundaries. The continuity is, of course, satisfied at the corner nodes of parent structure element containing the substructure by virtue of the application of assembly rules. Since the interface compatibility is not satisfied, a rigorous mathematical proof of an upper bound to the stiffness cannot be obtained. Nevertheless, the above procedure is being used increasingly because it usually provides useful engineering solutions.

NUMERICAL EXAMPLE

Consider a three-dimensional finite-element model of dimensions 24"x24"x36" as shown in Figure 14A. Because of

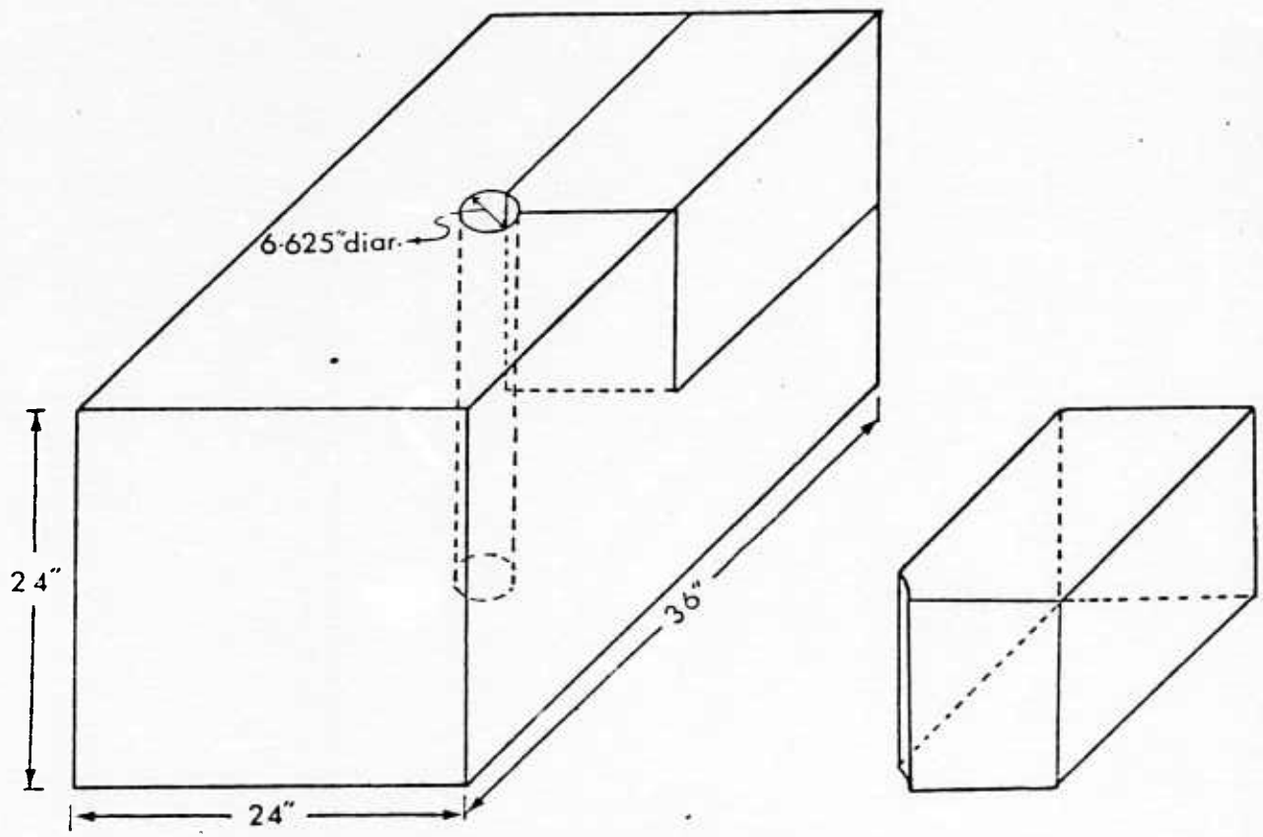

(a) Rectangular block model 24"x24"x36" (b) An octant of the model

Fig. 14 Numerical example - three-dimensional finite element model

symmetry, it is only necessary to consider an octant of the model as shown in Figure 14b. The geometry and material properties are given as follows:

Borehole diameter	= 6 5/8"
Trepanning hole diameter	= 1/4"
Young's modulus	= 8.57×10^6 psi
Poisson's ratio	= 0.191

The above geometry and material properties were chosen because they represent the rock block models of Redwood granite used to verify the proposed method of analysis.

The parent structure (Figure 15, is modeled into an assembly of 203 elements and the substructure (Figure 16) is further subdivided into 49 elements inter-connected at 130 nodal points. Nodes 3, 4, 5, 8, 9 and 10 are common to both parent and substructure. Six types of loading are applied to the parent structure. The strains at three gage points (Figure 17) around the trepanning hole are determined from substructure finite-element analysis and are summarized in Table 2

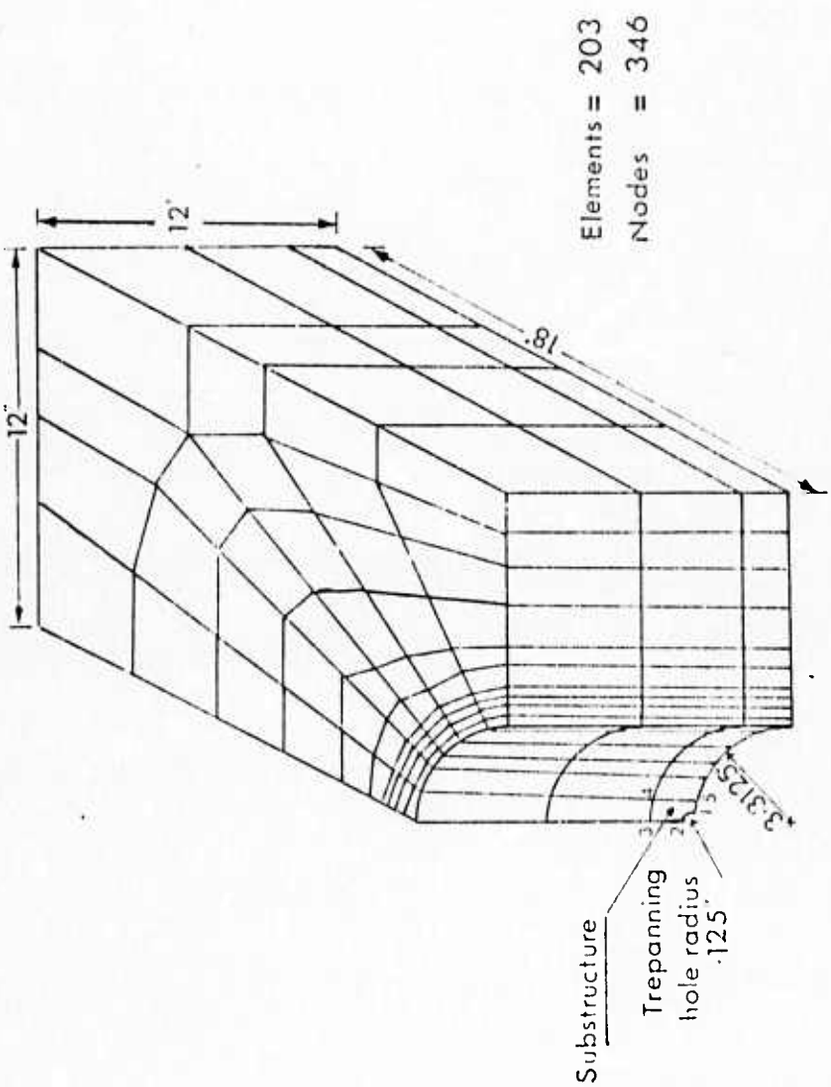

Fig. 15 The parent structure

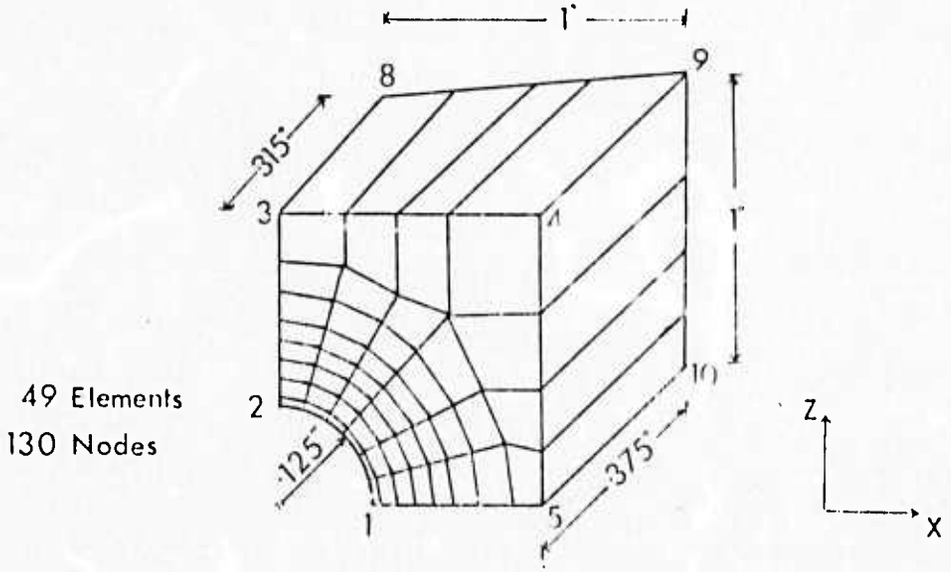

Fig. 16 The substructure

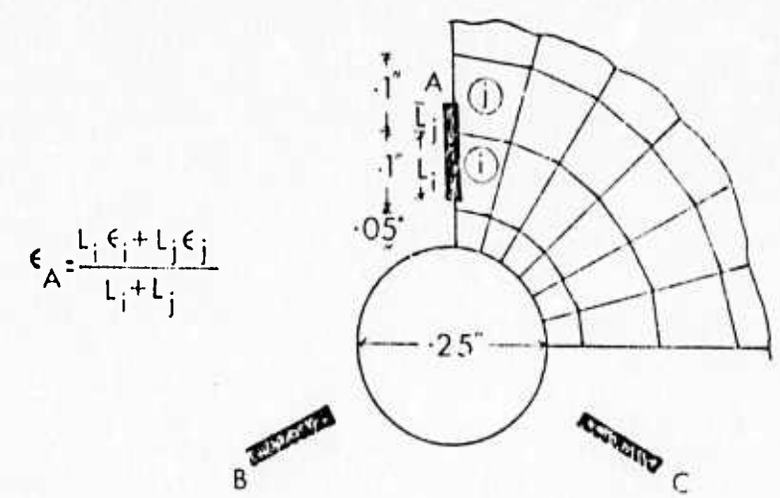

Fig. 17 The strain gage rosette around trepanning hole

TABLE 2 STRAINS AROUND TREPANNING HOLE

EXTERNAL LOAD (psi)	STRAINS (ε_t μin/in.) AROUND TREPANNING HOLE GAGE 1 (Vertical)	GAGE 2 (+120°)	GAGE 3 (-120°)
σ_x=+1	.01551	.1345	.1345
σ_y=+1	-.00517	-.0388	-.0388
σ_z=+1	.05208	.01654	.01654
τ_{xy}=+1	.2266	-.3277	.1581
τ_{yz}=+1	-.011987	.0497	.0071
τ_{zx}=+1	.0092	.0156	.2317

The strains at these three gage points in the absence of trepanning holes are obtained from a straight-forward, three-dimensional finite-element analysis and are given in Table 3

TABLE 3 STRAINS ON THE SIDEWALLS OF BOREHOLE

EXTERNAL LOAD (psi)	STRAINS ($-\varepsilon_b$ μin/in.) ON THE BOREHOLE WALLS GAGE 1 (Vertical)	GAGE 2 (+120°)	GAGE 3 (-120°)
σ_x=+1	-.07399	.1345	.1345
σ_y=+1	.02287	-.08181	-.08181
σ_z=+1	.1167	.01202	.01202
τ_{xy}=+1	.0231	-.08483	-.08483
τ_{yz}=+1	0	.03141	-.03141
τ_{zx}=+1	0	-0.2407	+0.2407

The relaxation strains are now obtained as the differences between the values listed in Tables 2 and 3 and are presented in Table 4. The three observation equations may now be written as

$$\begin{matrix} \varepsilon_{m1}^{(1)} \\ \varepsilon_{m2} \\ \varepsilon_{m3} \end{matrix} = \begin{matrix} \varepsilon_{r1}^{(1)} & \varepsilon_{r1}^{(2)} & \varepsilon_{r1}^{(3)} & \varepsilon_{r1}^{(4)} & \varepsilon_{r1}^{(5)} & \varepsilon_{r1}^{(6)} \\ \varepsilon_{r2}^{(1)} & \varepsilon_{r2}^{(2)} & \varepsilon_{r2}^{(3)} & \varepsilon_{r2}^{(4)} & \varepsilon_{r2}^{(5)} & \varepsilon_{r2}^{(6)} \\ \varepsilon_{r3}^{(1)} & \varepsilon_{r3}^{(2)} & \varepsilon_{r3}^{(3)} & \varepsilon_{r3}^{(4)} & \varepsilon_{r3}^{(5)} & \varepsilon_{r3}^{(6)} \end{matrix} \begin{matrix} {}^{(1)}\sigma_x \\ \sigma_y \\ \sigma_z \\ \tau_{xy} \\ \tau_{yz} \\ \tau_{zx} \end{matrix} \quad (3.25)$$

or $$\{\varepsilon_m\}^{(1)} = \{\varepsilon_r\}^{(1)}\{\sigma\} \quad (3.26)$$

TABLE 4 RELAXATION STRAINS DUE TO TREPANNING

EXTERNAL LOAD (psi)	RELAXATION STRAINS (ε_r μin/in.) DUE TO TREPANG. GAGE 1 (Vertical)	GAGE 2 (+120°)	GAGE 3 (-120°)
$\sigma_x = 1$	.0895	-.1376	-.1376
$\sigma_y = 1$	-.028	.043	.043
$\sigma_z = 1$	-.06462	.004516	.004516
$\tau_{xy} = 1$	.2035	-.2429	-.2429
$\tau_{yz} = 1$	-.011987	.01829	.03851
$\tau_{zx} = 1$	.0092	.2563	-.0091

where ε_{m1}, ε_{m2}, ε_{m3} are the relaxation strains measured at position (1) along z and $\pm 120^\circ$ directions.

Two more sets of equations of the above type can now be obtained for positions $\theta = 7\pi/6$ and $\theta = 11\pi/6$ by a simple transformation of components of stress. For the systems of axes OX'Y'Z' and OX"Y"Z" rotated through 120° in the counter-clockwise and clockwise directions respectively about Z-axis,

$$\{\varepsilon_m\}^{(2)} = \{\varepsilon_r\}^{(2)}\{\sigma\}' = \{\varepsilon_r\}^{(2)}(T)^{(2)}\{\sigma\} \qquad (3.27)$$

and $$\{\varepsilon_m\}^{(3)} = \{\varepsilon_r\}^{(3)}\{\sigma\}'' = \{\varepsilon_r\}^{(3)}(T)^{(3)}\{\sigma\} \qquad (3.28)$$

where $\{\varepsilon_m\}^{(2)}$ and $\{\varepsilon_m\}^{(3)}$ are the relaxation strain vectors measured at $\theta=7\pi/6$ and $\theta=11\pi/6$ positions respectively, and $\{\sigma\}'$ and $\{\sigma\}''$ are the stress components in OX'Y'Z' and OX"Y"Z" systems respectively. $(T)^{(2)}$ and $(T)^{(3)}$ are the coordinate transformation matrices and it can be shown that (10)

$$(T)^{(2)} = \begin{bmatrix} l_1^2 & m_1^2 & n_1^2 & 2l_1m_1 & 2m_1n_1 & 2n_1l_1 \\ l_2^2 & m_2^2 & n_2^2 & 2l_2m_2 & 2m_2n_2 & 2n_2l_2 \\ l_3^2 & m_3^2 & n_3^2 & 2l_3m_3 & 2m_3n_3 & 2n_3l_3 \\ l_1l_2 & m_1m_2 & n_1n_2 & (l_1m_2+l_2m_1) & (m_1n_2+m_2n_1) & (n_1l_2+n_2l_1) \\ l_2l_3 & m_2m_3 & n_2n_3 & (l_2m_3+l_3m_2) & (m_2n_3+m_3n_2) & (n_2l_3+n_3l_2) \\ l_3l_1 & m_3m_1 & n_3n_1 & (l_3m_1+l_1m_3) & (m_3n_1+m_1n_3) & (n_3l_1+n_1l_3) \end{bmatrix} \qquad (3.29)$$

where the direction cosines l, m, n between the primed and unprimed coordinate axes are defined in the following table:

	X	Y	Z
X'	l_1	m_1	n_1
Y'	l_2	m_2	n_2
Z'	l_3	m_3	n_3

From the above table we see that l_1=Cos X'X, m_2=Cos Y'Y etc.

An equation similar to (3.29) may be written for $(T)^{(3)}$.

For the problem under consideration, the transformation tables of direction cosines are

	X	Y	Z
X'	-1/2	$\sqrt{3}/2$	0
Y'	$-\sqrt{3}/2$	-1/2	0
Z'	0	0	1

and

	X	Y	Z
X"	-1/2	$-\sqrt{3}/2$	0
Y"	$\sqrt{3}/2$	-1/2	0
Z"	0	0	1

Substituting these values in the expressions for $(T)^{(2)}$ and $(T)^{(3)}$ and combining equations (3.26), (3.27) and (3.28), we obtain

$$\{\varepsilon_m\} = (A)\{\sigma\} \tag{3.30}$$

where $\{\varepsilon_m\}$ is a 9x1 vector corresponding to measured relaxation strains at three θ-positions and (A) is given by

$$(A)=\begin{bmatrix} .0895 & -.028 & -.06462 & .2035 & -.1199 & .0092 \\ -.1376 & .043 & .004516 & -.2429 & .0183 & .2563 \\ -.1376 & .043 & .004516 & .2429 & .0385 & -.0091 \\ .0895 & -.028 & -.06462 & -.2035 & .0679 & .0992 \\ -.1073 & .0127 & .004516 & .2778 & .2128 & -.1441 \\ .1030 & -.1976 & .004516 & .0349 & -.0271 & -.0288 \\ .0895 & -.028 & -.06462 & .0016 & .052 & -.1084 \\ .1030 & -.1976 & .004516 & -.0349 & .2311 & -.1123 \\ -.1073 & .0127 & .004516 & -.2778 & -.1146 & .0378 \end{bmatrix} \tag{3.31}$$

Thus nine equations are obtained to determine the six

unknown stress components. From this overdetermined set of equations one can solve for the stresses $\{\sigma\}$ by either of the two methods already described in the previous sections. The set of equations (3.30) thus represent the necessary equations to determine the stress tensor in any linearly elastic, isotropic and homogeneous rock at any depth in the earth's crust from the strain measurements on the sidewalls of deep boreholes.

Following the development of a new three-dimensional method for the determination of primary stresses in rock, an experimental investigation has been planned to verify some of the results of the analysis. The experimental program is presented in the next section.

EXPERIMENTAL STUDIES

INTRODUCTION

A program was established for testing large rock block models whereby the maximum amount of information could be obtained from the minimum number of tests. The program was developed to satisfy two specific goals:

(1) To verify the adequacy of the model components that had been developed; namely model material, loading apparatus and instrumentation.

(2) To yield information on the response of a limited number of models at the borehole-trepanning hole intersection so that the results may be compared with the numerical solution obtained in the previous chapter.

Two kinds of tests were carried out on two different rectangular block models of the same material. The difference between the two models results from different borehole orientation and loading with reference to borehole axis. Nevertheless exactly the same scheme and sequence of loading were used for both models.

Strain gage rosettes were placed at selected locations on the sidewall of the borehole. The rosettes were mounted on the blocks so that one strain gage was parallel (or nearly parallel) to the borehole axis. This selected

orientation of gages allowed for relatively easier comparison between the experimental and theoretical values.

Both models were loaded incrementally up to a pressure of 500 psi. Increments of 50 psi were used for all tests. Incremental loading allowed time for the scanning and recording of the strain values and pressure from the measuring devices. The tests were all repeated at least six times in order to minimize statistical fluctuations and obtain consistent results.

ROCK TYPE, LOCALE AND MATERIAL PROPERTIES

Two blocks of Precambrian Milbank Granite were obtained from a quarry near Redfield, South Dakota. A detailed geolgic description of Milbank granite is given by Daniells(1971) and White(1973). The general geologic relationships and petrographic details of the Milbank granite have been described by Goldich (1961) Hall (1899) and Theil and Dutton (1935)

The Milbank granite is a medium- to coarse-grained light reddish brown rock. It consists of coarse-grained, pink microcline, coarse- to medium-grained white orthoclase, medium-grained, bluish-gray quartz, dark brown fine-grained biotite and minor amounts of plagioclase. A few feldspar grains are found to be larger than the prevalent grain size.

In thin section, the rock is holocrystalline, phaneritic, medium- to coarse-grained and inequiangular. Large grains of orthoclase and microcline are characteristically surrounded by fine-grained, granulated quartz and orthoclase. The rock consists of 37% anhedral, irregular, fine- to medium-grained quartz, 51% anhedral, medium- to coarse-grained microcline, 10% anhedral, coarse-grained plagioclase, fine-grained, irregular biotite grains scattered throughout the rock mass, and traces of magnetite and apatite. The minerals do not seem to be preferentially oriented; they contain numerous small fractures both at and across grain boundaries.

Daniells(1971)has determined the material properties of Milbank granite from unconfined compression tests on 1 7/8" diameter cylindrical specimens in the laboratory. The rock is isotropic and has an unconfined compressive strength of 23,000 psi. The modulus of elasticity and Poisson's ratio of the material are determined to be 8.57 x 10^6 psi and 0.191 respectively.

DESCRIPTION OF THE MODELS AND EXPERIMENTAL SET UP

The details of the models and the experimental set up are shown in Figures 18 and 19 Figure 18a shows the first model of Milbank granite of dimensions 24"x24"x36" with a cylindrical hole of 6 5/8" diameter in the middle of

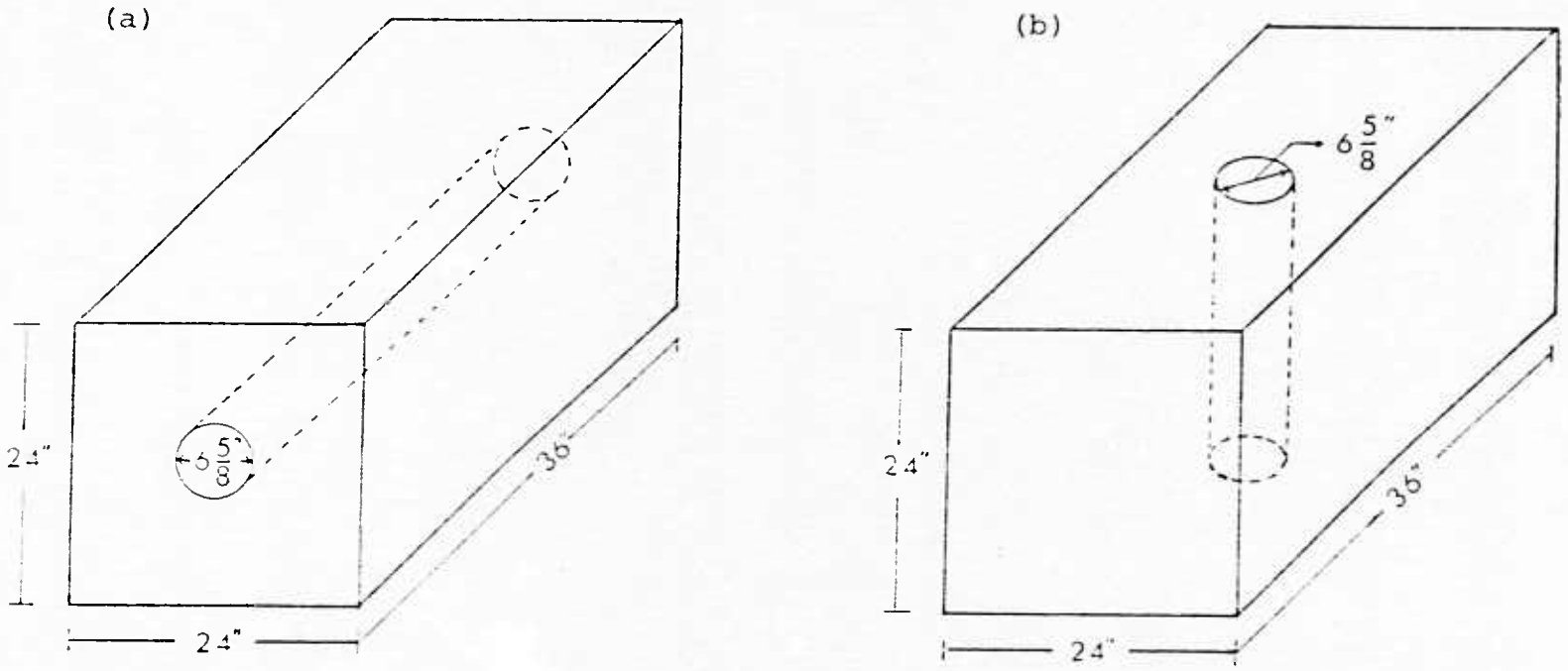

Fig. 18a Milbank granite rock block model 1

Fig. 18b Milbank granite rock block model 2

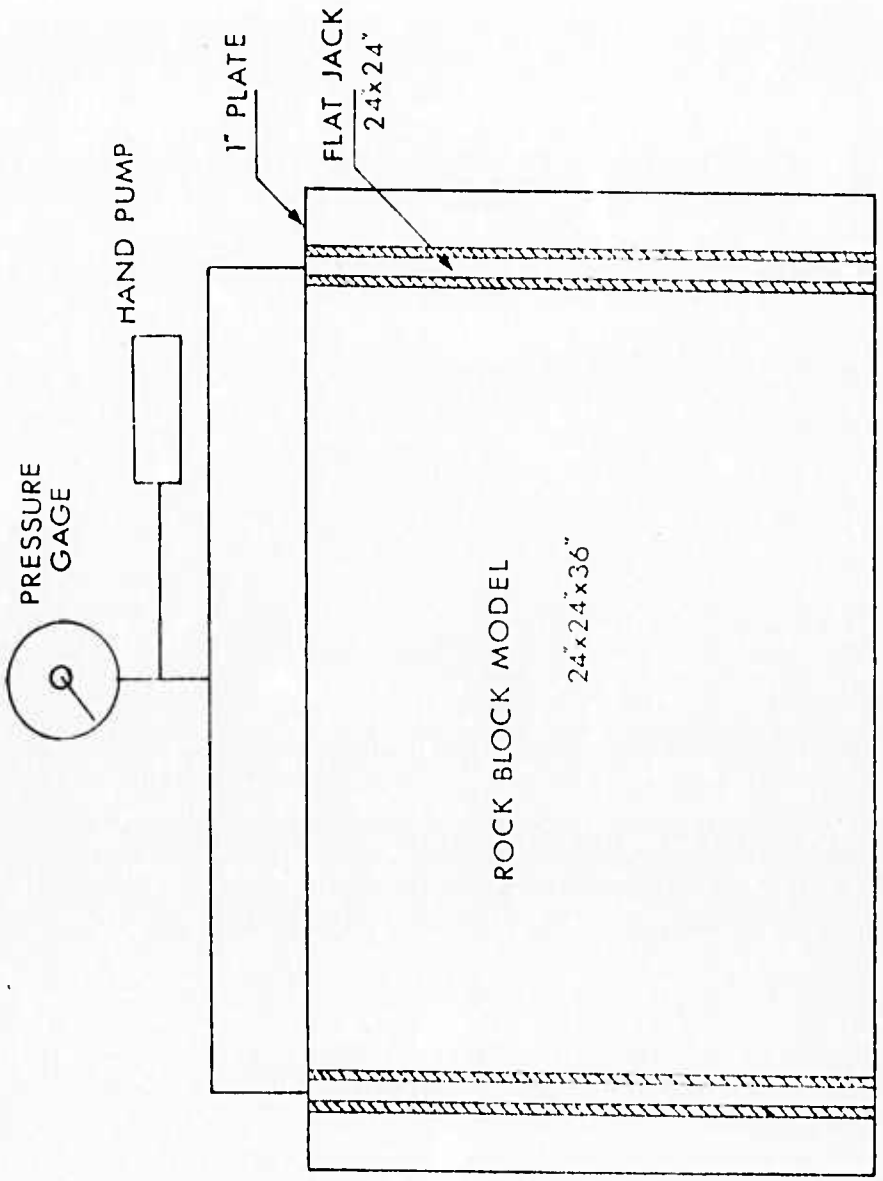

Fig. 19 Schematic diagram of loading apparatus and rock block model

square face. The second model has identical overall dimensions but the cylindrical hole is drilled in the middle of one of the rectangular faces. These two models were loaded in uniaxial compression by a loading frame as shown in Figure 19 This loading frame is similar to the one used by Hoskins(1967) for uniaxial compressive loading of rock and concrete blocks.

The loading frame consisted of two steel end plates held at a fixed distance by threaded rods of 3" diameter. Eight rods and bolts were used to tie the two end plates together. The end plates were 1-inch thick mild steel plates with three wide flange W8x40 beams 24" long welded to the outside faces of the end plates. The I-beams were stiffened by welding 1/2 in. thick plates cut to shape into the webs at each end of each beam. The middle I-beam at one end of the frame had a 7" pipe in the middle and was concentric with the 6 5/8" cylindrical hole in the first rock model. Large flat hydraulic jacks (24"x24") with and without circular cut-outs were used to load the rock and these jacks acted against the relatively rigid frame. The flat jacks were sandwiched between two 1/4 in. sheets of masonite packing material to obtain a uniform stress application to the model.

MODEL PREPARATION AND TESTING PROCEDURE

The models were large blocks of dimensions 24 in. x 24 in. x 36 in., and the instrumentation was installed after fitting the model into the loading frame as shown in Figure 19 A 1/4 in. hole was drilled to a depth of 1/2" on the borehole walls of the two models at a distance of 4" from the block boundary. In model 2, the hole was drilled in a direction normal to the loading axis. Both strain gage rosettes (120° delta) and single element gages were used to measure strains on the borehole walls and around the 1/4 in. holes. The gages were all 1/8 in. long.

All 120 degree rosettes used were Micro Measurements (M-M) precision strain gages, type EA-06-125YA-120 with a gage factor of 2.065 ±1% and a resistance of 120 ohms ±0.2%. The single element gages were M-M precision strain gages, type EA-06-125BT-120 with a gage factor of 2.11 ±0.5% and a resistance of 120 ohms ±15%. The compensating gage was also of this type. The gages were all open-faced general purpose gages with a polyimide backing.

Strain gage rosettes were installed on the borehole walls at locations diametrically opposite to the 1/4 in. holes. Three single-element gages were installed around each 1/4 in. hole. These three single gages constitute a single strain rosette. The rosette configuration chosen

for tests on models 1 and 2 are shown in Figures 20 and 21 It may be seen that the strain gages were all placed at a distance of 1/16" from the hole boundary. Since the strain gradient around a hole of this size was comparatively steep, it was necessary to devise a means of accurately positioning the strain gages. Flexible paper templates were designed for this purpose. Both the hole and the positioning of strain gages were accurately drawn on the template which was then cut along the hole circumference and gage boundaries (Figure 22). The strain gages were positioned in the slots and then carefully attached to the template by taping along their boundaries. The lead wires were next soldered on to the gage terminals and the entire unit was mounted on the rock surface.

The strain gages were installed on the rock surface using M-Bond 200, a methyl-2-cyanoacrylate adhesive and M-Bond 200 catalyst. Because of its easy handling and immediate room temperature cure, this adhesive proved to be very satisfactory. A coating of Dow Corning 3140 RTV, a clear, non-corrosive, flowable, room temperature curing silicone rubber, was applied over the strain gages and terminal strips for moisture resistance and to avoid gage instability and any mechanical damage.

Before bonding the strain gage on the borehole wall,

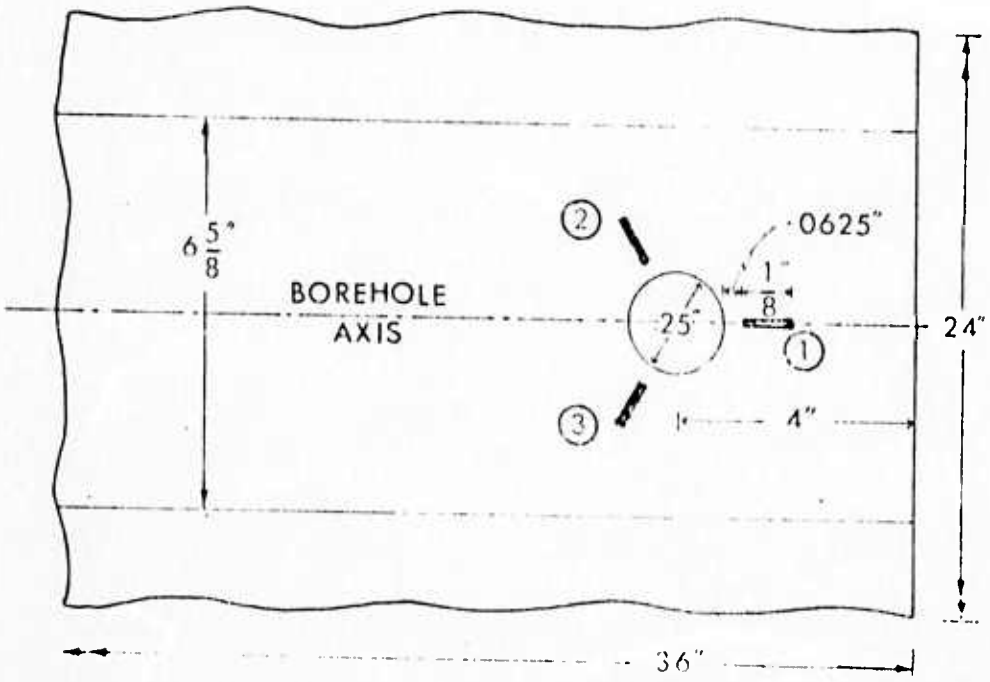

Fig. 20 Trepanning hole rosette configuration in model 1

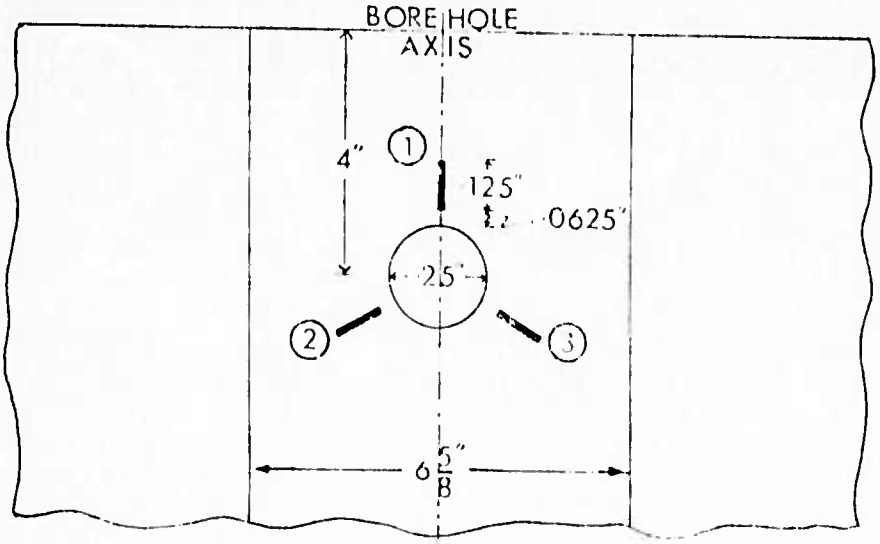

Fig. 21 Trepanning hole rosette configuration in model 2

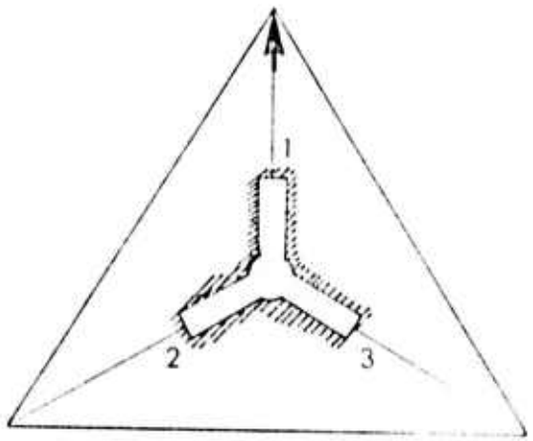

Fig. 22 Paper template for positioning gages

it was necessary to prepare the rock surface. The surface was first sanded and then thoroughly cleaned with acetone. A generous spray of Freon degreaser followed. The rosette gages were then bonded to the surface with the M-Bond 200 adhesive and catalyst. Excessive adhesive was forced from under the gages by pressing on the gages from the center outward. This reduced the possibility of air bubbles being present under the gages. Immediately upon completion of wipe-out of the adhesive, firm thumb pressure was applied to the gages and terminal area for several minutes after which the gages were solidly bonded in place. The gages were then visually checked for improper bonding. Gage-to-gage specimen resistance was measured with a multimeter to make sure the gages were intact.

An identical gage bonded in the same way to a separate block of material was used as the temperature compensating gage. Only one compensating gage was used throughout the experimental work.

Two types of strain indicators were used to record strain readings. A Bean Model 201 Digital Strain Indicator in association with a 5-channel Model 301 switch and balancing unit were used. Both indicators proved stable and reproducibility of strain readings was good.

Two flat jacks were used to apply normal

stress to the models. Pressure was applied to each jack by a 3000 psi hand pump. The pressure applied by the hand pump was monitored by the previously calibrated 5000 psi pressure gage.

The lead wires from the strain gages were connected to the strain indicators. The indicators were then connected to power supplies and allowed to warm up for a period of several minutes. During the warm up time, all the connections were checked. Another check on the pressure gage and pressure valve was made.

The initial strain values of all strain gages were checked and recorded. Pressure was then applied through the hand pump in 50 psi increments. At each increment, the strain values of all strain gages were recorded. The process was continued until a pressure of 500 psi was applied. Then the pressure was released gradually until it was brought back to zero. The strain values were again recorded at every 50 psi pressure drop during unloading process. The loading and unloading cycle was repeated at least six times and the final strain values are calculated by averaging the 12 sets of readings so obtained.

COMPARISON AND DISCUSSION OF RESULTS

The average strain values obtained from models 1 and 2 are presented in Tables 4 and 5 The difference

TABLE 5

STRAIN VALUES AT THREE GAGE LOCATIONS FOR MODEL 1

Pressure (psi)	Strains on the Sidewall (μin/in.)			Strains Around Trepanning Hole (μin/in.)			Relaxation Strains (μin/in.)		
	$\varepsilon_1(0^\circ)$	$\varepsilon_2(+120^\circ)$	$\varepsilon_3(-120^\circ)$	$\varepsilon_1(0^\circ)$	$\varepsilon_2(+120^\circ)$	$\varepsilon_3(-120^\circ)$	$\varepsilon_1(0^\circ)$	$\varepsilon_2(+120^\circ)$	$\varepsilon_3(-120^\circ)$
0.	0.	0.	0.	0.	0.	0.	0.	0.	0.
-50.	-4.33	-1.0	-1.0	-2.33	-2.00	-2.0	2.00	-1.0	-1.0
-100.	-9.50	-1.0	-1.0	-4.67	-3.0	-3.0	4.83	-2.0	-2.0
-150.	-14.25	-2.0	-2.0	-6.25	-3.0	-3.0	8.00	-1.0	-1.0
-200.	-19.67	-2.0	-2.0	-8.0	-4.0	-4.0	11.67	-2.0	-2.0
-250.	-25.33	-3.0	-3.0	-10.0	-5.0	-5.0	15.33	-2.0	-2.0
-300.	-30.00	-3.0	-3.0	-12.33	-6.0	-6.0	17.67	-3.0	-3.0
-350.	-35.00	-4.0	-4.0	-14.00	-6.0	-6.0	21.00	-2.0	-2.0
-400.	-39.33	-4.0	-4.0	-16.25	-8.0	-8.0	23.08	-4.0	-4.0
-450.	-44.50	-4.0	-4.0	-18.33	-8.0	-8.0	26.17	-4.0	-4.0
-500.	-50.00	-5.0	-5.0	-20.0	-10.0	-10.0	30.0	-5.0	-5.0

Note: + denotes extension; - contraction

TABLE 6

STRAIN VALUES AT THE THREE GAGE LOCATIONS FOR MODEL 2

Pressure (psi)	Strains on the Sidewall (μin/in.)			Strains Around Trepanning Hole (μin/in.)			Relaxation Strains (μin/in.)		
	$\varepsilon_1(0\pm)$	$\varepsilon_2(120\pm)$	$\varepsilon_3(120\mp)$	ε_1(v)	$\varepsilon_2(+120^o)$	$\varepsilon_3(-120^o)$	ε_1(v)	$\varepsilon_2(+120^o)$	$\varepsilon_3(-120^o)$
0.	0.	0.	0.	0.	0.	0.	0.	0.	0.
-50.	1.5	-8.33	-5.33	-1.17	-3.50	0.	-2.94	3.36	6.96
-100.	3.0	-22.33	-15.67	-1.50	-6.67	-6.33	-4.99	12.58	12.92
-150.	6.0	-45.83	-25.83	-2.34	-22.33	-21.67	-10.63	14.65	15.31
-200.	9.0	-80.47	-33.17	-3.51	-30.00	-31.17	-20.31	30.72	29.55
-250.	11.33	-107.08	-45.47	-5.34	-36.83	-33.85	-26.66	44.44	45.42
-300.	15.33	-116.00	-54.67	-5.83	-42.47	-43.17	-29.92	47.25	46.55
-350.	18.00	-137.33	-66.50	-6.34	-50.33	-51.51	-34.2	56.51	55.33
-400.	19.50	-154.50	-77.50	-7.50	-58.33	-57.67	-37.35	62.84	63.5
-450.	21.33	-172.00	-85.83	-8.51	-69.33	-70.00	-41.36	65.34	64.67
-500.	25.00	-184.67	-93.50	-10.17	-75.33	-74.67	-47.18	70.42	69.76

between the strains around the hole and the corresponding strains measured at a diametrically opposite point gives the relaxation strains at these points. Therefore the 1/4 in. hole is termed a trepanning hole although no rosette was undercored. This procedure also eliminates any residual stresses present in the rock and allows a direct comparison to be made between the experimental results and predicted values.

From Table 5 it may be seen that the response of the gages is linear. The values in the first three columns are the strains resulting from a homogeneous compressive stress field. For an applied stress (σ_z) of 500 psi along the borehole axis, the principal stresses and strains computed from experimental values using elastic stress-strain relationships are compared (Table 7) with Hiramatsu's elasticity solution (1962)and three-dimensional finite-element solution. Both theoretical solutions give identical results which is, of course, expected for this simple uniaxial compressive field. The experimental values show good agreement in general. However, the discrepancy is as large as 15% for minimum stress and strain values. This can be partly accounted for by the fact that relatively small strains were measured and the strain indicator readings can only be estimated within $\pm$ 2.5 microinches/inch. Therefore

any small discrepancy in the measured strains will result in a very large percentage for smaller measured strains.

TABLE 7

COMPARISON BETWEEN EXPERIMENTAL AND THEORETICAL SOLUTIONS (MODEL 1, MEASUREMENTS ON SIDEWALL), p=500 psi

Principal Stresses and Strains	Experimental	Hiramatsu's Solution	3D-FEM
σ_{max}	+4.0	0	0
σ_{min}	-427.74	-500.0	-500.0
ε_{max}	-10.00	-11.14	-11.14
ε_{min}	-50.0	-58.34	-58.34

The strains measured around the trepanning hole in model 1 are given in columns 4 to 6 of Table 5 By subtracting the corresponding strains in columns 1 to 3 from these values, the relaxation strains were obtained and are shown in columns 7 to 9. The relaxation strains at the three gage points were also predicted by performing a three-dimensional substructure finite-element analysis on model 1. The theoretical strains were computed by taking weighted averages over the elements on which the gages were placed. Predicted strain values versus measured strain values are shown in Figure 23 It can be seen that the experimental values lie very close to the predicted values for gage 1. The agreement is quite good for gages 2 and 3 but the percentage discrepancy is large at some discrete points.

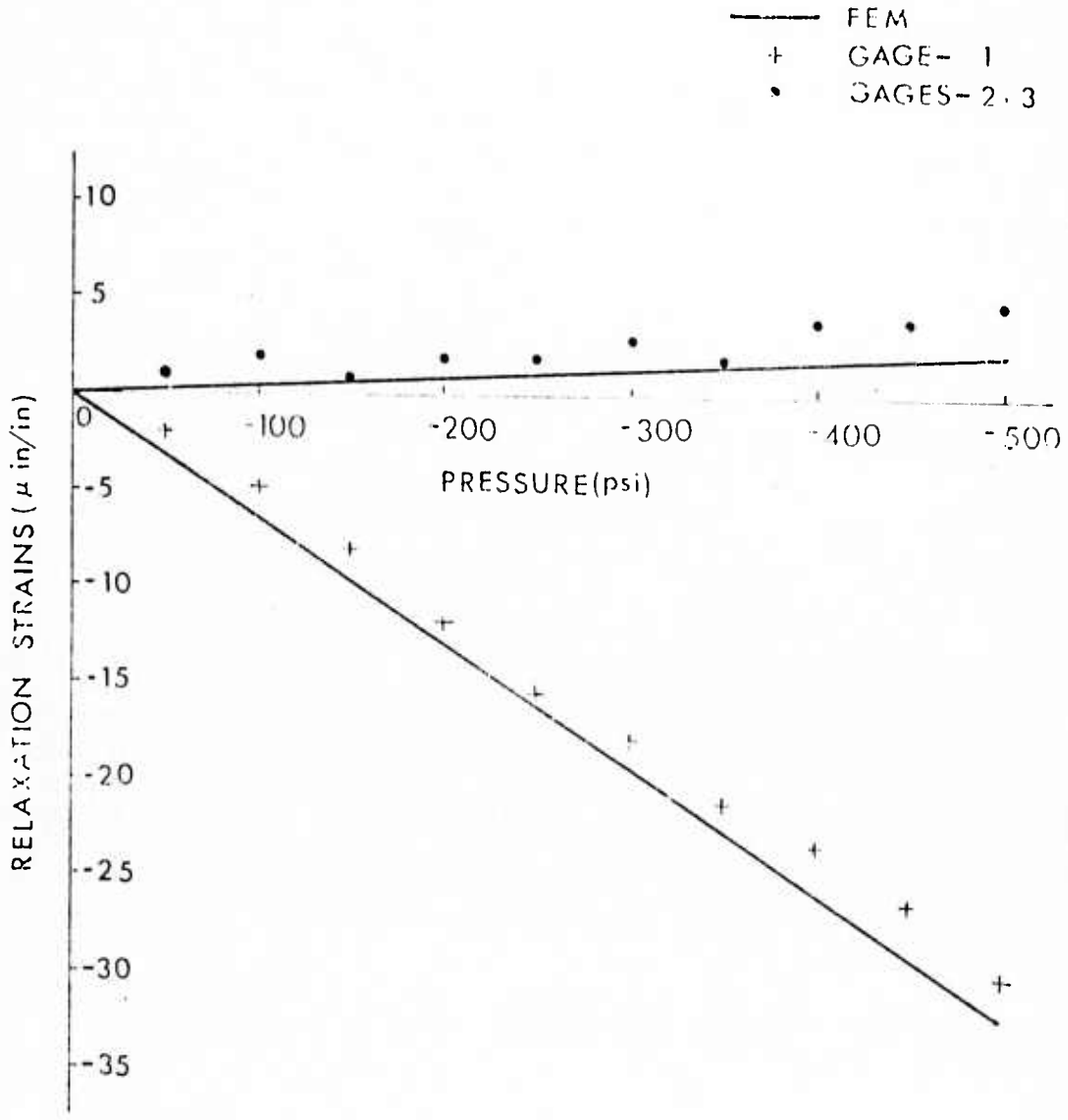

Fig. 23 Comparison between experimental and predicted relaxation strains for model 1

experimental values.

From the experimental relaxation strain values, the applied stress field was calculated using Russell's two-dimensional data reduction computer program for deep hole device. The stresses along and normal to the borehole axis were found to be -487 psi and -27 psi respectively. To obtain the applied stress field from the three-dimensional analysis, a total of nine relaxation strain measurements were required whereas only three measurements were made. Since the model is subjected to a uniform homogeneous compressive stress field, the same three relaxation strains should exist at each and every θ-position, if there are no statistical fluctuations in the experimental values. Using equation (3.24b) with a unit weight matrix and equation (3.31), the principal stresses were found to be equal to -486 psi, -23 psi and -23 psi. The agreement is excellent since the difference in the applied stress field (σ_z=500 psi) is only 2.4%.

In testing model 2, the linear response of the model in the designed loading range was first verified by the strains measured on the sidewall of the borehole. Figure 24 shows the response of strain rosette to the uniaxial compressive stress applied normal to the borehole axis. The dispersion of strains for any single gage clearly

As already mentioned, this is mainly because of the very small strain values.

In addition to discrepancies due to differences in recording smaller strains, discrepancies could have been introduced due to any of the following causes:

(1) Inaccuracies in determining the elastic constants. The predicted strains are dependent on the Young's modulus and Poisson's ratio of the material. So, any change in these values directly affects the strains.

(2) The measurements were made at points not very far from the outside boundary of the block of rock. This was necessary to make the drilling process simple and accurate, but the ideal location would be within the middle third portion of the model.

(3) The rock satisfies the homogeneity condition only in a statistical sense. Any of the gages may cover a particular crystal whose elastic constants differ from those of the model material.

(4) Another possible source of error may be due to the inadequacy of the finite-element model. Because of the limitation imposed by the computer core storage, models with a much finer subdivision were not investigated. A finer mesh or a model with refined (higher order) elements might result in a much closer agreement with the

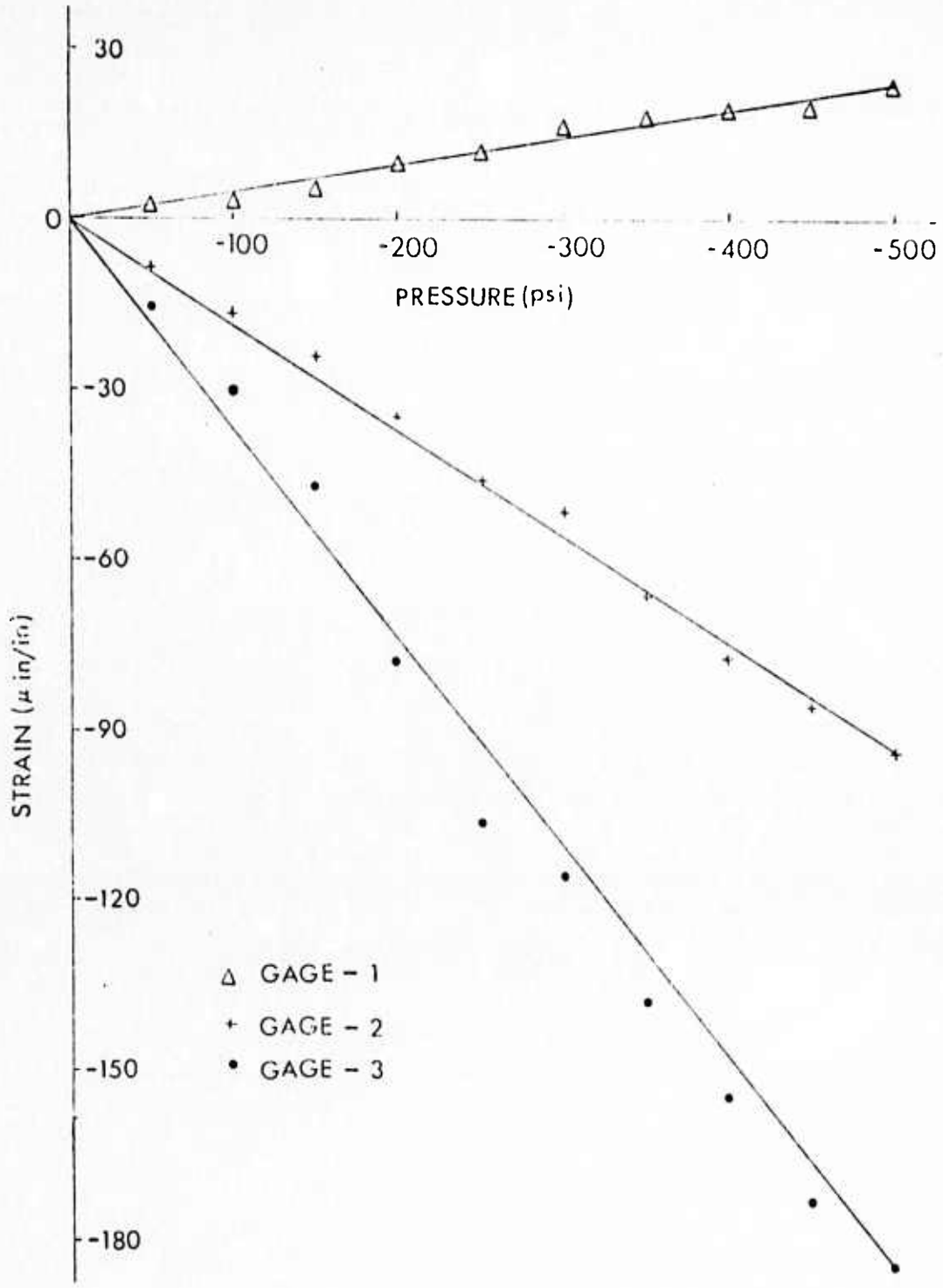

Fig. 24 Response of strain rosette to uniaxial compression perpendicular to borehole axis (model 2)

indicates a linear trend.

From the strain values in the first three columns of Table 6 the principal stresses, strains and their directions were determined using the equations derived in Appendix B. If gage 1 was made to coincide with the direction of the borehole axis, the maximum principal strain direction would be 0° with reference to gage 1. But the gage was inclined at approximately 15° to the borehole axis, and with an applied compressive stress σ_x=-500 psi, the maximum principal strain direction was found to be equal to $-12^{\circ}53'$ (clockwise negative). The principal strain direction was determined for every set of strain readings and the results were plotted as shown in Figure 25 From this figure, it may be seen that the principal strain direction does not show a variation of more than $\pm 2^{\circ}$ which proves that the strains were highly consistent and responded linearly to the applied stress field.

For an applied compressive stress field of 500 psi, the principal stresses and strains on the sidewalls of a borehole were computed using Howland's solution (1930) Hiramatsu's three-dimensional elasticity solution (1962) and three-dimensional finite-element solution. In Table 8 these results are presented along with experimentally determined values. Howland's two-dimensional elasticity

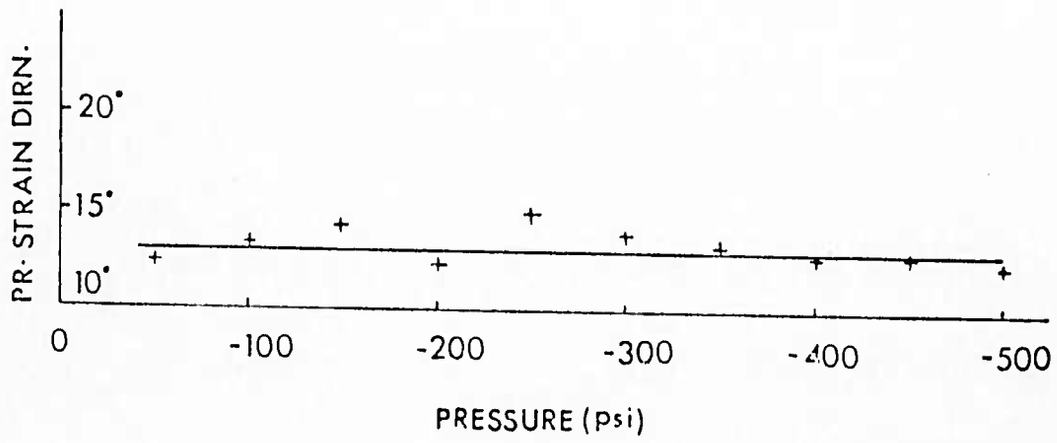

Fig. 25 Variation of principal strain direction with pressure (model 2, no hole)

solution for a semi-infinite strip.

TABLE 8

COMPARISON BETWEEN EXPERIMENTAL AND THEORETICAL SOLUTIONS

(Model 2, Measurements on Sidewall, p=-500 psi)

Principal Stresses and Strains	Experimental	Howland	Hiramatsu	3D-FEM
σ_{min}(psi)	-1767.49	-1660.0	-1500.	-1664.0
σ_{max}(psi)	-20.45	-	0	-5.21
σ_{min}(psi)	-205.79	-193.70	-179.68	-194.72
σ_{max}(psi)	+37.01	-	+21.70	+36.5

under tension and the three-dimensional finite-element solutions show the closest agreement with the experimentally determined values. The maximum principal stress and strain values cannot be obtained from Howland's solution which is two-dimensional. Hiramatsu's solution which is valid only if the block may be regarded as indefinitely extended in two dimensions, gives a principal stress value of -1500 psi corresponding to a stress concentration factor of 3.0. Both Howland's solution and finite-element solution give a somewhat higher stress concentration factor of 3.3 at this point. The three-dimensional finite-element solution shows excellent agreement with the experimentally determined values, the difference being less than 6% in all but one case.

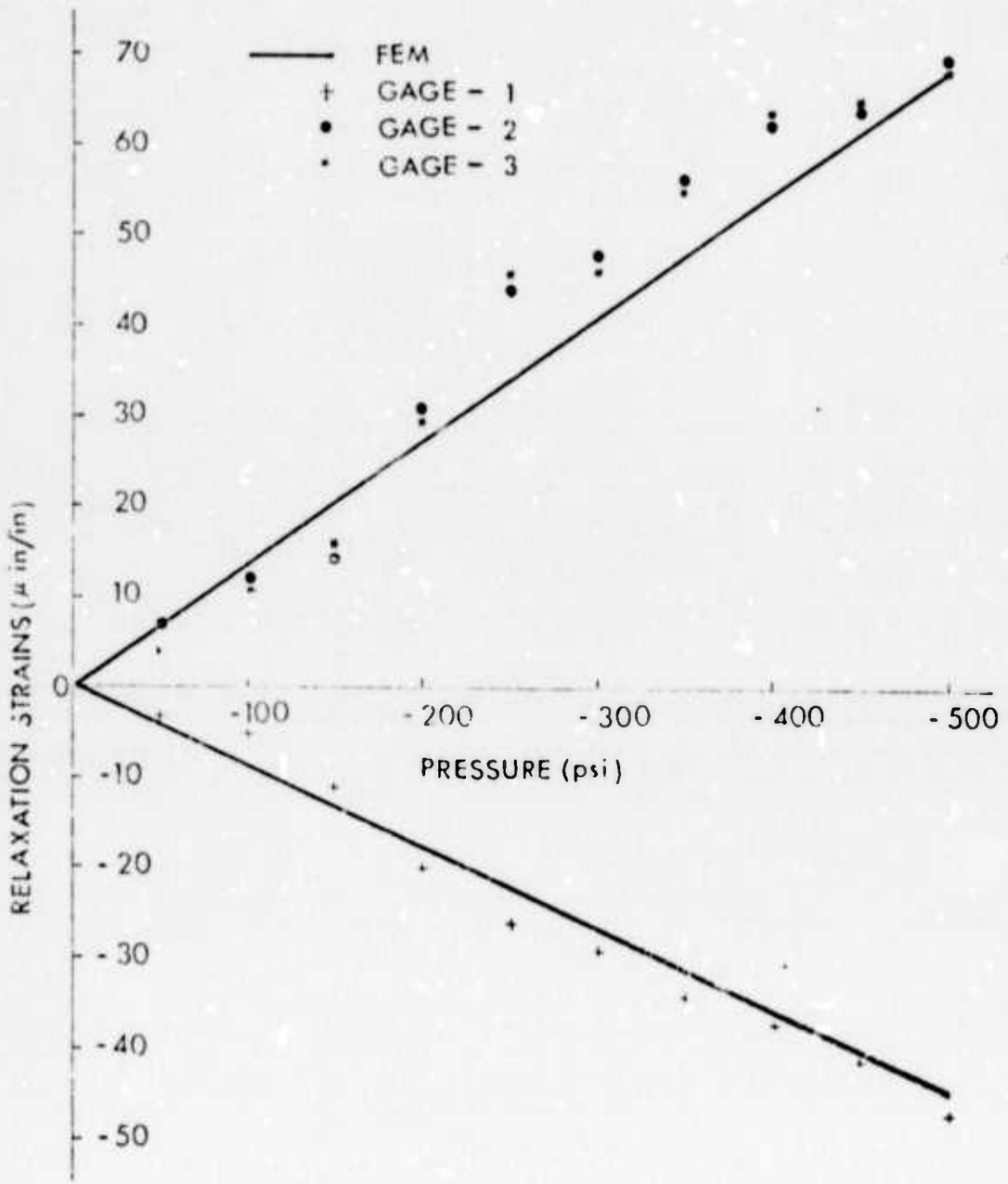

Fig. 26 Comparison between experimental and predicted relaxation strain model 2

The strains around the trepanning hole are shown in columns 4 to 6 of Table 6 For obtaining the relaxation strains for model 2, the strains along vertical and $\pm 120^{\circ}$ directions had to be computed because of the positioning of the rosette at this location. The relaxation strains thus obtained from experimental values were plotted against the values predicted by the three-dimensional substructure finite-element analysis in Figure 26 The theoretical values were once again determined by taking weighted averages of the strains in elements over which the gages were placed. Very good agreement has been found and the differences seldom exceed $\pm 15\%$.

CONCLUDING REMARKS

The results of the experimental investigation have confirmed the application of three-dimensional substructure analysis presented in the previous chapter for determining primary stresses in rock from measurements on the sidewalls of boreholes. This has been demonstrated by the excellent agreement between the experimental and theoretical values of the relaxation strains in the tested models. With the experimental set up that was used and the magnitudes of strains that were measured, agreement between theoretical and experimental values within ± 10 to 15% would be considered acceptable. From the values presented in Tables 7

and 8 and Figures 23 and 26, it may be pointed out that the differences between experimental and theoretical values are less than $\pm$10% in a majority of cases.

ANALYTICAL METHOD

The purpose of this section is to describe the results of an investigation into a suitable means of converting the nine components of relieved strain into principal stresses. These stresses are assumed to act a point in the center of the hole at the depth of the device prior to drilling the borehole and the trepanning holes. A further objective of the analysis is to provide information useful in designing an efficient device. It is assumed that the mechanical properties of the rock in the region of the measurement will be known from either laboratory tests on core cut from the borehole or from a device capable of measuring mechanical properties in place.

Assumptions In order to estimate the stress field at a point that existed prior to drilling the borehole and the trepanning holes, a number of assumptions are made. These assumptions may be divided into those inherent in the strain relief system and those made to simplify the analysis of the data.

Assumptions inherent in the strain relief method and device are 1) strain changes resulting from residual stresses are negligible in comparison with those due to gravity, active tectonic forces and any other forces presently acting, (Residual stresses are defined as those acting in a body of rock in the absence of any external force or force field), 2) stress gradients are small enough so that they cause only negligible changes in strain over the dimensions used in the device, in other words, the difference in stress between the highest and lowest strain gage units is negligible in comparison with the total stress, 3) strain gages bond to continuous rock and do not span significant voids or joints and 4) the device anchoring jacks, bonding of the strain gages and drilling of the holes do not significantly alter the behavior of the rock in the neighborhood of the measurement, i.e., tests for mechanical properties run on cores should be representative

of the in situ rock.

Assumptions made to simplify the analysis are 1) the rock in the neighborhood of the trepanning holes may be modeled as a linear isotropic, homogeneous elastic material, 2) any inelastic effects that may occur very close to the holes are not significant, 3) the trepanning holes act independently, i.e., drilling the first trepanning hole does not affect the results from drilling the second and third holes, 4) the curvature of the borehole may be neglected in computing the principal stresses from the relieved strains and 5) the direction parallel to the borehole is a principal direction. Assumption number 4, neglect of borehole curvature in comparison with trepanning hole diameter, allows us to use the two-dimensional plane stress solution for determing stresses from relieved strains.

Method Using the above assumptions, an approximate solution may be found by the following procedure:
1) Analyze the strain relief for each strain gage unit by using a modification of a method published by Soete (1950).
2) Check the results from the three trepanning holes for consistency in the vertical stress in accordance with assumption 5 above, if assumption 5 is satisfied, proceed with the analysis, otherwise, the approximate analysis

fails,

3) Since the direction of the borehole is a principal direction, the second and third principal directions at each trepanning hole must lie in a plane normal to the axis of the borehole, therefore, we have the tangential component of stress at three points around the circumference of the borehole spaced at 120 degrees and assumed to be acting in the same plane,

4) Since the vertical stress (assumed not to vary with X and Y) can be shown to have no effect on the horizontal stress distribution, the three tangential stresses at 120 degrees are sufficient to determine the two principal stresses and the principal direction in the horizontal plane. In the next two sections, the modified Soete method and the principal stresses in the horizontal plane are developed.

Strain Relief Near a Trepanning Hole The stress and strain fields existing in a material will be disturbed by the drilling of a trepanning hole. The change in the strain field near the hole can be measured by means of electrical resistance strain gages or some other suitable means. The basic relationship between the original strain field, the change in strain and the final strain field may be expressed by the following equation.

Final Strain Field = Original Field + Change in Field (1)

Since strain gages measure only an average strain over their length and not the entire strain field, we can rearrange Eq. 1 and interpret it to hold at any point in the strain field. Then for any point,

Measured Strain = Final Strain - Original Strain (2)

where measured strain has been equated with the average change in strain over the length of the strain gage used.

If we assume that stress gradients will produce only negligible changes in stress over the dimensions involved, the 2-D state of stress in the borehole wall (assumed to be a plane) may be expressed in terms of two principal stresses and a principal angle. Similarly, the final state of stress around the trepanning hole may be expressed in terms of the same principal stresses and angle by using the 2-D plane-stress solution originally developed by Kirsch (1898). Since we are neglecting the curvature of the borehole for the analysis of the strain relief at the trepanning holes, we are essentially on the surface of a half-space where the normal component of stress is zero. Consequently, the plane stress solution is the appropriate approximation.

The above argument implies that the measured strain

at a point near a trepanning hole may be expressed as a function of two principal stresses and a principal angle acting in a plane normal to the axis of the trepanning hole. Thus

$$\text{Measured Strain} = \text{Function}\ (\sigma_1,\ \sigma_2,\ \theta) \tag{3}$$

where σ_1 and σ_2 are the principal stresses and θ is the principal angle all acting in a plane normal to the axis of the trepanning hole being considered. As shown below the function implied by Eq. 3 is nonlinear. Therefore, if we apply Eq. 3 to each of the three strain gages around a trepanning hole, we will have a set of three simultaneous, nonlinear, algebraic equations which may be used to solve for the three unknowns σ_1, σ_2 and θ acting near the trepanning hole.

In equation form, from Soete (1950), we have

$$\varepsilon'_0 = A_0\ V_1 + B_0\ V_2\ V_3 \tag{4a}$$

$$\varepsilon'_{+\alpha} = A_{+\alpha}\ V_1 + B_{+\alpha}\ V_2 \cos\ 2(\theta+\alpha) \tag{4b}$$

$$\varepsilon'_{-\alpha} = A_{-\alpha}\ V_1 + B_{-\alpha}\ V_2 \cos\ 2(\theta-\alpha) \tag{4c}$$

where α is the angle between gages as shown on Fig. 3,

$$V_1 = (\sigma_1+\sigma_2)/E \tag{5a}$$

$$V_2 = (\sigma_1-\sigma_2)/E \tag{5b}$$

$$V_3 = \cos(2\theta) \tag{5c}$$

E = Young's modulus of elasticity

ε'_m = average measured strain

$$= \frac{1}{r_{m_2}-r_{m_1}} \int_{r_{m_1}}^{r_{m_2}} \varepsilon'_{rm}\,dr \quad \text{(used to develop Eqs. (4) \& (6),}$$

where m = 0, $+\alpha$, and $-\alpha$,

r_{m_1} and r_{m_2} are respectively the radial distances from the center of the hole to the inner and outer edges of the strain gage grid at angle m,

ε'_{rm} is the function representing the variation of the radial strain with the radial coordinate, r, at the angle m,

$$A_m = \frac{1+\nu}{E} \frac{a^2}{r_{m_1} r_{m_2}} \tag{6a}$$

$$B_m = \frac{2a^2}{r_{m_1} r_{m_2}} \left\{-1 + \frac{(1+\nu)}{4} \cdot \frac{a^2 (r^2_{m_1} + r_{m_1} r_{m_2} + r^2_{m_2})}{r^2_{m_1} r^2_{m_2}}\right\} \tag{6b}$$

m = 0, $+\alpha$, $-\alpha$, and

a = radius of trepanning hole.

Note that the function representing the variation of radial strain is averaged only over the radial direction, this implies that the width of the strain gage grid must be small in comparison with the radius of the trepanning hole.

The three unknowns in Eqs. 4 are V_1, V_2, and V_3. If the three values of V are known, we can easily solve for σ_1 σ_2 and θ. Before proceding with the solution, the cosine terms in Eqs. 4b and 4c must be expressed in terms of $V_3 = \cos 2\theta$. This can be accomplished by using standard trigonometric identities. Then

$$A_o V_1 + B_o V_2 V_3 = \varepsilon'_o \tag{7a}$$

$$A_{+\alpha} V_1 + B_{-\alpha} V_2 (V_3 \cos 2\alpha - \sqrt{1-V_3^2} \sin 2\alpha) = \varepsilon'_{+\alpha} \tag{7b}$$

$$A_{-\alpha}V_1+B_{-\alpha}V_2(V_3\cos 2\alpha+\sqrt{1-V_3^2}\sin 2\alpha)=\varepsilon'_{-\alpha} \qquad (7c)$$

Since the right hand sides of Eqs. 7 are the measured changes in strain at the three angles and all of the symbols on the left hand side, except the three V's, can be computed from a knowledge of the material properties and the geometry, Eqs. 7 constitute a set of three simultaneous, nonlinear, algebraic equations in terms of the three unknown values of V.

Eqs. 7 differ from those presented by Soete (1950). Soete assumed that each strain gage was at exactly the same distance from the center of the trepanning hole. In that case, the three A's in Eqs. 7 could be represented by a single symbol A'. Similarly, the three B's in Eqs. 7 could be represented by B'. The simpler geometry allows the direct solution of the equations and is given by Soete. As will be shown later, the principal stresses are very sensitive to small changes in geometry. Therefore, a solution was constructed for the more general Eqs. 7.

To construct a solution to Eqs. 7, we first add Eq. 7b and Eq. 7c to eliminate the square root term. The product V_2V_3 remains but can be eliminated by using Eq. 7a to give

$$V_1=\frac{\varepsilon'_{+\alpha}+\varepsilon'_{-\alpha}-\bar{B}\varepsilon'_o}{A_{-\alpha}+A_{-\alpha}-\bar{B}A_o} \qquad (8a)$$

where $\bar{B} = (B_{+\alpha}+B_{-\alpha})\cos(2\alpha)/B_o$

An expression may be obtained for V_2 by first subtracting Eq. 7c from Eq. 7b and then eliminating

V_3 by using Eq. 7a. After some algebraic manipulation,

$$V_2 = \{\frac{(A_{-\alpha}-A_{-\alpha})V_1-(\varepsilon'_{-\alpha}-\varepsilon'_{-\alpha})^2}{\bar{B}\tan 2\alpha} + (\varepsilon'_o-A_oV_1)^2\}^{\frac{1}{2}}/B_o \quad (8b)$$

The remaining unknown V_3 may be found from Eq. 7a to be

$$V_3 = (\varepsilon'_o-A_oV_1)/(B_oV_2) \quad (8c)$$

It should be noted that Eqs. 8 must be solved sequentially since the expression for V_2 involves V_1 and the expression for V_3 involves both V_1 and V_2. Algebraic substitutions could be made but the sequential calculation causes no difficulty and appears to be the most efficient way of obtaining numerical values for the unknowns.

After calculating the values for V_1, V_2 and V_3, Eqs. 5 are used to find

$$\sigma_1 = E(V_1+V_2)/2 \quad (9a)$$

$$\sigma_2 = E(V_1-V_2)/2 \quad (9b)$$

$$\theta = \pm 1/2 \cos^{-1}(V_3) \quad (9c)$$

The correct sign for the principal angle θ may be found by substituting into either Eq. 4b or 4c. If the equation is satisfied, the correct sign has been chosen for θ. The angle θ is defined as the clockwise angle measured from the direction of principal stress σ_1 to the direction chosen as 0. It should be noted that the equations derived above assume that tension is positive. Also, the σ derived in the above equations may not be the algebraic maximum principal stress.

Principal Stresses in 3D. The strain change data from each of the three trepanning holes are analyzed using Eqs. 8 and

and 9. As previously stated, if the results from each trepanning hole do not indicate that the vertical direction is principal, the approximate method fails and a more exact approach must be taken, see Sateesha (1974). It is anticipated that in the majority of practical situations, the vertical direction will be vertical and the average of the three vertical stress components from the three trepanning holes will be an adequate representation of the magnitude of the vertical principal stress. At this stage we know one principal direction is vertical and it follows that the remaining two principal directions are in the horizontal plane. It remains for us to solve for the two principal stress magnitudes and one principal angle in the horizontal plane. From the analysis of the three trepanning holes, tangential stresses are now known at three points around the circumference of the borehole as shown on Fig. 27

Again the problem may be solved by using the Kirsch solution

$$\sigma_t = (p_1+p_2)-2(p_1-p_2)\cos 2\beta \qquad (10)$$

where σ_t is a tangential component of stress at the borehole surface, p_1 and p_2 are principal stresses acting in the horizontal plane prior to drilling (tension positive) and β is the principal angle measured clockwise from the direction of p_1 to the reference direction 0. If we denote the three known tangential stress components at the borehole surface as σ_{to}, $\sigma_{t+\gamma}$, $\sigma_{t-\gamma}$ where γ is generally 120 degrees, and apply the Kirsch solution three times, we have

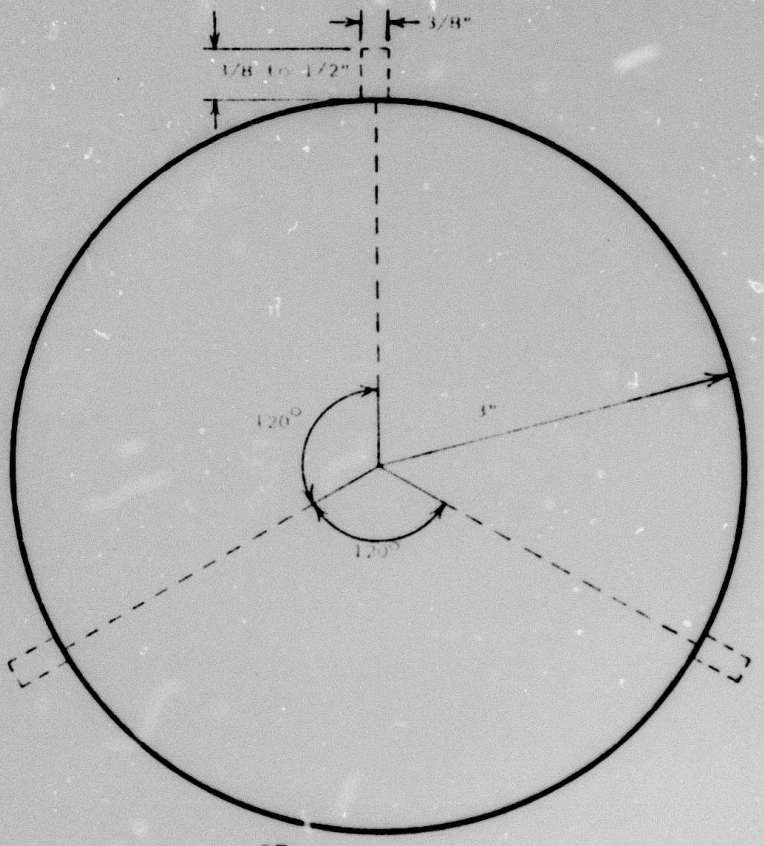

Fig 27 Cross section of borehole

$$\sigma_{to} = U_1 - 2U_2U_3 \tag{11a}$$

$$\sigma_{t+\gamma} = U_1 - 2U_2\cos 2(\beta+\gamma) \tag{11b}$$

$$\sigma_{t-\gamma} = U_1 - 2U_2\cos 2(\beta-\gamma) \tag{11c}$$

where

$$U_1 = P_1 + P_2 \tag{12a}$$

$$U_2 = P_1 - P_2 \tag{12b}$$

$$U_3 = \cos 2\beta \tag{12c}$$

Eqs. (11) have exactly the same form as Eqs. (4) if we make the following associations

$U_i \rightarrow V_i$ $\quad i = 1, 2, 3$ $\qquad \sigma_{to} \rightarrow \varepsilon'_o$

$1 \rightarrow A_m$ $\qquad \sigma_{t+\gamma} \rightarrow \varepsilon'_{+\alpha}$

$-2 \rightarrow B_m$ $\qquad \sigma_{t-\gamma} \rightarrow \varepsilon'_{-\alpha}$

$\gamma \rightarrow \alpha$

$\beta \rightarrow \theta$

Using Eqs. 8 and the above associations, the solution to Eqs. (11) is

$$U_1 = \frac{\sigma_{t+\gamma} + \sigma_{t-\gamma} - 2\cos 2\gamma}{2(1-\cos 2\gamma)} \tag{13a}$$

$$U_2 = -\left\{\left(\frac{\sigma_{t-\gamma} - \sigma_{t-\gamma}}{2\sin 2\gamma}\right)^2 + (\sigma_{to} - U_1)\right\}^{1/2}/2 \tag{13b}$$

$$U_3 = (U_1 - \sigma_{to})/(2U_2) \tag{13c}$$

From Eqs. (12), the principal stresses and angle in the horizontal plane are

$$P_1 = (U_1+U_2)/2 \tag{14a}$$

$$P_2 = (U_1-U_2)/2 \tag{14b}$$

$$\beta = \pm\tfrac{1}{2}\cos^{-1}(V_3) \tag{14c}$$

The appropriate sign for β may be found by substituting β with an assumed sign into Eq. (11b) or Eq. (11c), if the correct sign is assumed, the equation is satisfied.

RESULTS

Verification of Results The above equations for determining principal stresses can be checked for algebraic consistency by assuming a stress field, computing the corresponding changes in strain from Eqs. 4 and then proceeding through the analysis as though these were actual measured strains. If the equations are consistent, the original stress field should be recovered. This algebraic check has been performed but will not be presented here in order to conserve space.

The algebraic check gives no information on the validity of the assumptions inherent in the method. These assumptions can be checked by either performing a more exact analysis and comparing results or by attempting to verify the results experimentally. Sateesha (1974) has performed a limited experimental study in the laboratory. A block of Milbank Granite 2 ft. x 2 ft. in cross-section and 3 ft. long was drilled leaving a 6 inch diameter borehole parallel to the 3 ft. dimension. The block was placed in a specially designed loading frame and loaded parallel to the borehole with a pressure of 500 psi.

Strain gages placed on the borehole wall approximately 6 inches from the end registered the longitudinal and tangential components of strain. The block was then unloaded and a ¼ inch diameter trepanning hole was drilled into the borehole wall. The block was again loaded and the strains around the trepanning hole were recorded. The difference between the strain readings without the trepanning hole and those with the hole were taken to be the change in strain that would have been recorded if the trepanning hole had been drilled while the block was under load. The advantage of the above experimental procedure is that residual stresses are eliminated from the strain changes. This is important since the strain level is relatively low due to the low stress level and the relatively high modulus of elasticity of the granite used.

Results obtained from the test are shown on Table 9 The agreement shown is relatively good and the discrepancies are well within the tolerances of the strain measurements and the material properties.

	Applied Stress (psi)	Stress Computed from Measured Strain Changes (psi)
σ_z	500	487
σ_x	0	27
σ_y	0	27

Table 9 Comparison of applied stresses with those computed from measured strain changes.

The results from one laboratory test certainly do not verify all the assumptions inherent in the technique itself or the approximate method of analysis. For example, the question of what is the smallest ratio of borehole diameter to trepanning hole diameter for which the neglect of the borehole curvature is appropriate has not been answered. Nevertheless, the results are sufficiently encouraging to warrant further study of the equations to determine the sensitivity of the results to errors in Poisson's ratio and gage pattern geometry.

Sensitivity and Error Analysis

As noted in the introduction, one of the objectives of this study is to provide meaningful input to the design process. One of the basic questions that arises in the design of the device concerns the most efficient size of trepanning hole that is practical and what size of strain gage should be used in conjunction with the trepanning

hole. If the problem is viewed from the instrumentation point of view, it is apparent that a relatively large signal is desired in order to minimize the inevitable noise problems in transmitting the signal from the device to a recorder at the surface. Consequently, an efficiency appropriate to this situation can be defined as the ratio of strain relieved in a particular direction (usually vertical) by trepanning to the maximum strain that could occur in that direction in a uniaxial test, σ/E. Taking a vertical stress of 1000 psi and a horizontal stress of 250 psi and maintaining a constant distance between the edge of the hole and the inner edge of the strain gage grid of 1/16 inch, relieved strains have been calculated for various hole diameters and strain gage grid lengths using Eqs. 4. The results of Efficiency vs. Grid Size/Hole Diameter are shown on Fig. 28 Fig. 28indicates that for maximum efficiency the ratio of grid size to hole diameter should be as small as possible. This is reasonable since a strain gage averages the strain over its length and the distribution of radial strain is nonlinear with the highest values occurring adjacent to the hole. The efficiencies shown hold only for the value of Poisson's ratio used and the fixed clearance between the strain gage grid and the edge of the hole. Nevertheless, the conclusion seems to

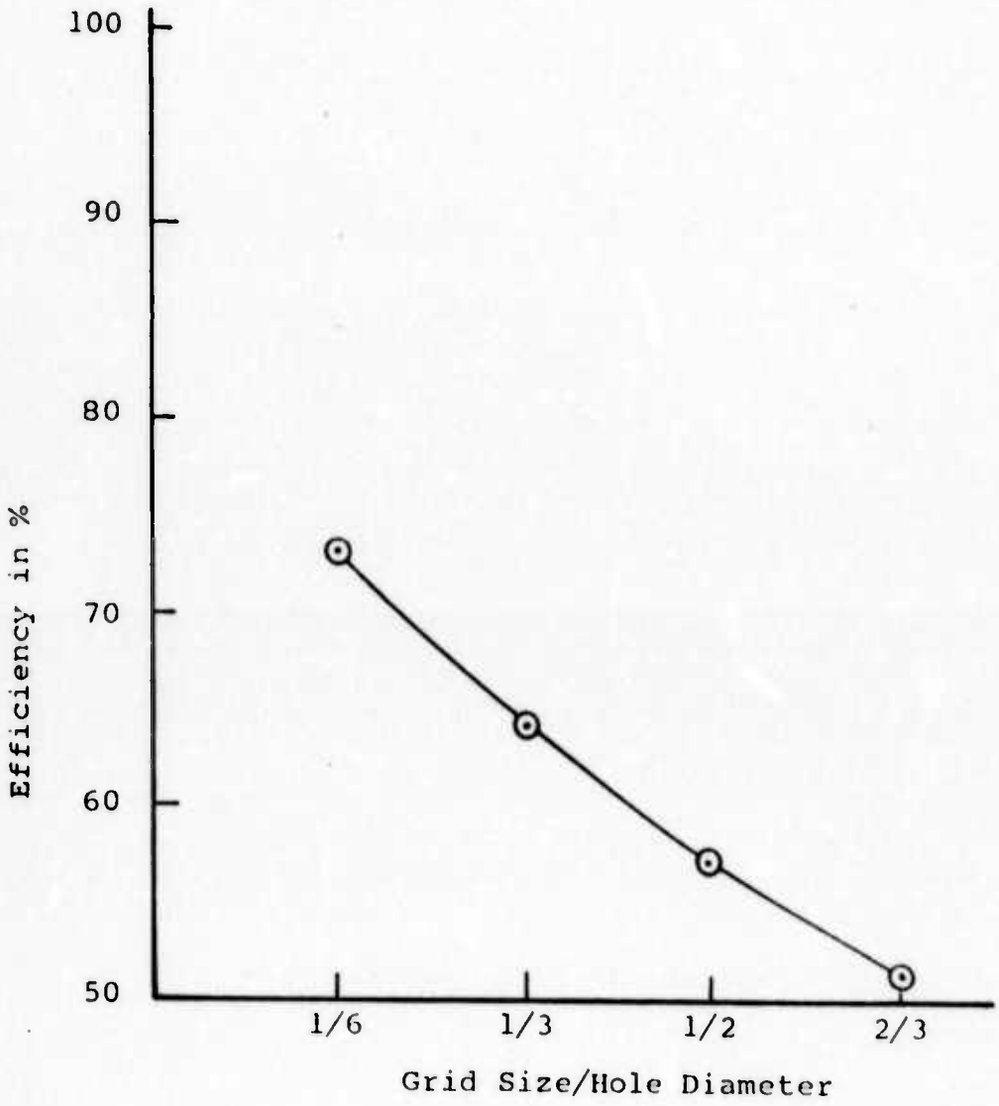

Fig. 28 Efficiency vs. grid size/hole diameter

be warranted and the values approximate for the practical situation. A ratio of grid size to hole diameter of 1/6 would coincide to a 1/16 inch grid and a hole diameter of 6/16 = 3/8 inch. For a nominal borehole of 6 inch diameter, these values of trepanning hole diameter and strain gage grid size are perfectly reasonable although practical constraints on the friction bonding strain gages may preclude the use of these relatively small gages.

Another question worthy of consideration relates to how sensitive the computed stresses are to errors in the strain gage pattern radius. Assuming the same stress field as noted above, the per cent error in vertical and horizontal components of stress may be computed for the assumed correct position of the strain gages and for gage pattern radii differing from the assumed by various amounts. The results are presented on Fig. 29 which shows the relative error in the horizontal and vertical components of stress versus error in the gage pattern radius. The results are based on the assumption that each of the three strain gages is placed the same distance from the center of the hole. Fig. 29 essentially shows that the results in terms of stress are relatively sensitive to errors in the strain gage pattern radius and that the horizontal components of stress are more sensitive than the vertical component.

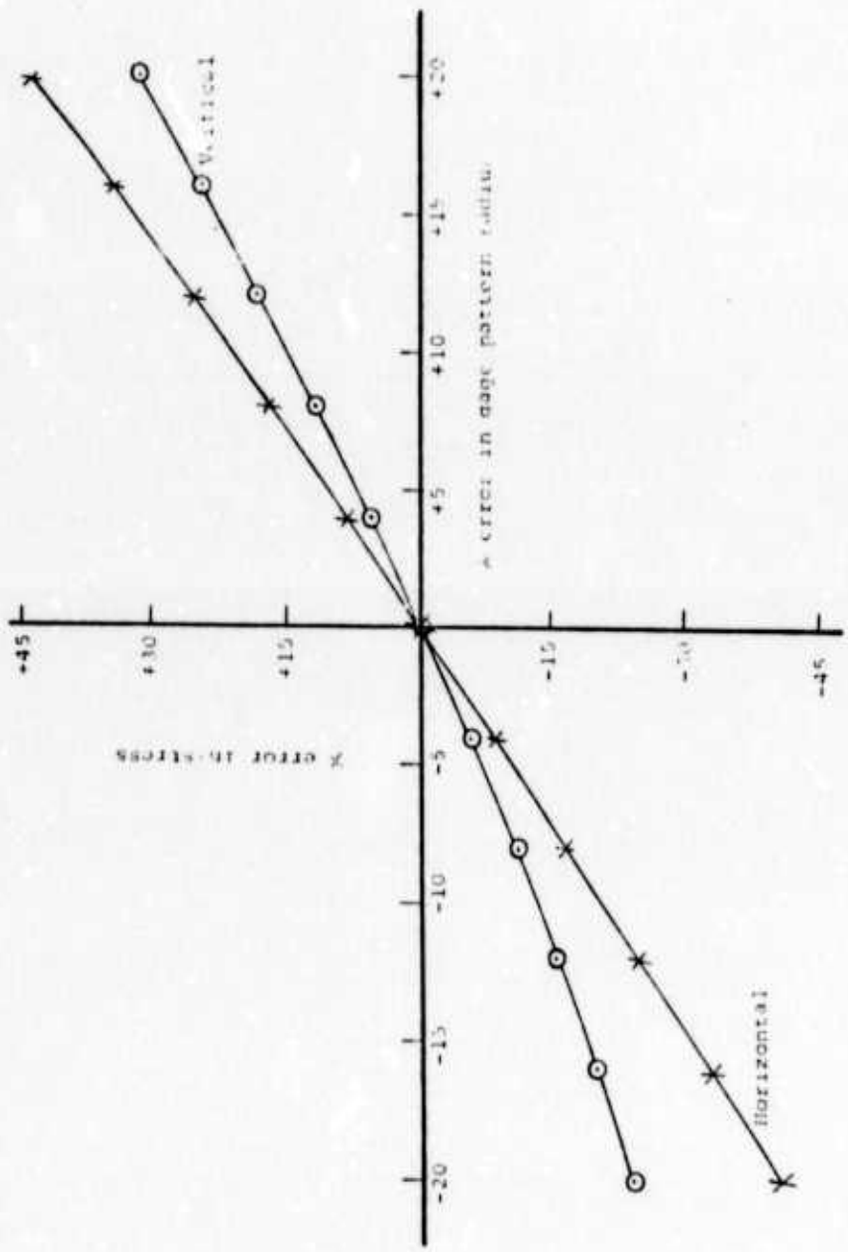

Fig. 29 % error in stress vs. error in gage pattern radius

Consequently care must be taken in the device to measure accurately the radius of the strain gage pattern.

The relatively high sensitivity of the stress components to changes in the gage pattern radius leads one to question the sensitivity of the stresses to an error in the placement of one of the gages in the pattern. The vertical gage was chosen for study since it probably represents the worst condition if not accurately placed. Again the same nominal stress field was chosen and the position of the vertical gage was changed while the two gages at $\pm$ 120 degrees were maintained at a constant radius. Fig.30 shows the per cent error in the vertical and horizontal components of stress that would result for various errors in the placement of the vertical gage. It is noted that the vertical component of stress is much more sensitive to errors in th placement of the vertical gage than the horizontal components of stress are. Again we note that great attention should be paid to the positioning of the strain gages in the pattern and the exact measurement of the pattern prior to testing.

Another potential source of error in the determination of stress components from relieved strains involves the accuracy of the material properties determined from core. Since the equations show that the components of stress

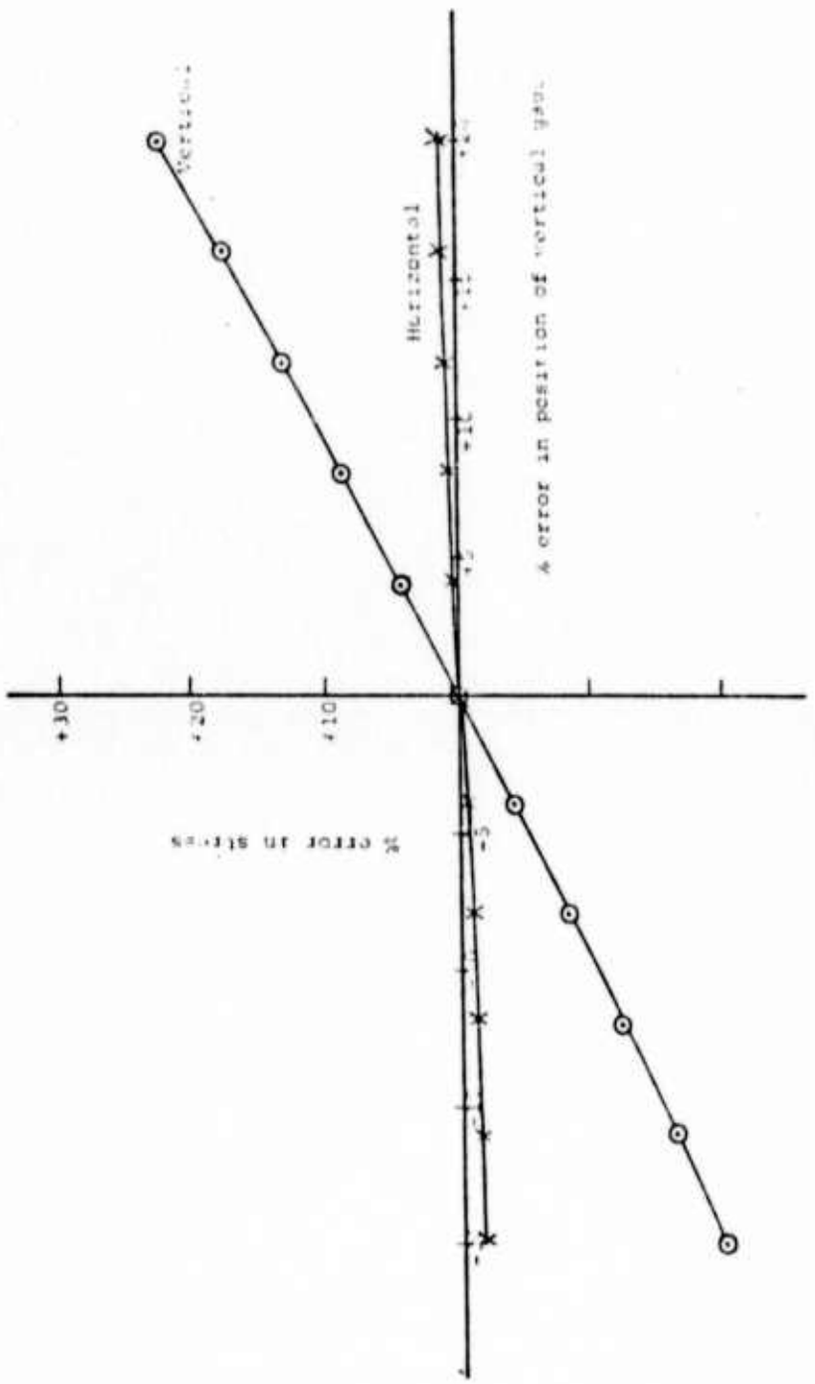

Fig. 30 Sensitivity to error in position of vertical gage

may be made dimensionless by dividing by Young's modulus, any error in the modulus will be reflected directly in the stress components. The situation is not so straight forward when considering the effect of errors in Poisson's ratio. The previously derived equations may be used to study the effect of changes in Poisson's ratio on the components of stress starting again with a vertical stress of 1000 psi and a horizontal stress of 250 psi which implies in the perfectly elastic situation that Poisson's ratio is 0.2. Fig.31 shows the error in stress components versus error in Poisson's ratio. Vertical stress is less sensitive to the error than horizontal stress although neither is very sensitive. For example, an error of 25% in Poisson's ratio leads to an error of 2.5% in the vertical stress and approximately 7% in the horizontal stress.

CONCLUSIONS

An approximate analysis of strain relief data from a deephole trepanning device is possible. This approximate analysis is based on a modified version of the Soete method in conjunction with the Kirsch solution. The solution presented is restricted to the case where the vertical direction is a principal direction. An extension of the approach presented here to a more general 3D stress field

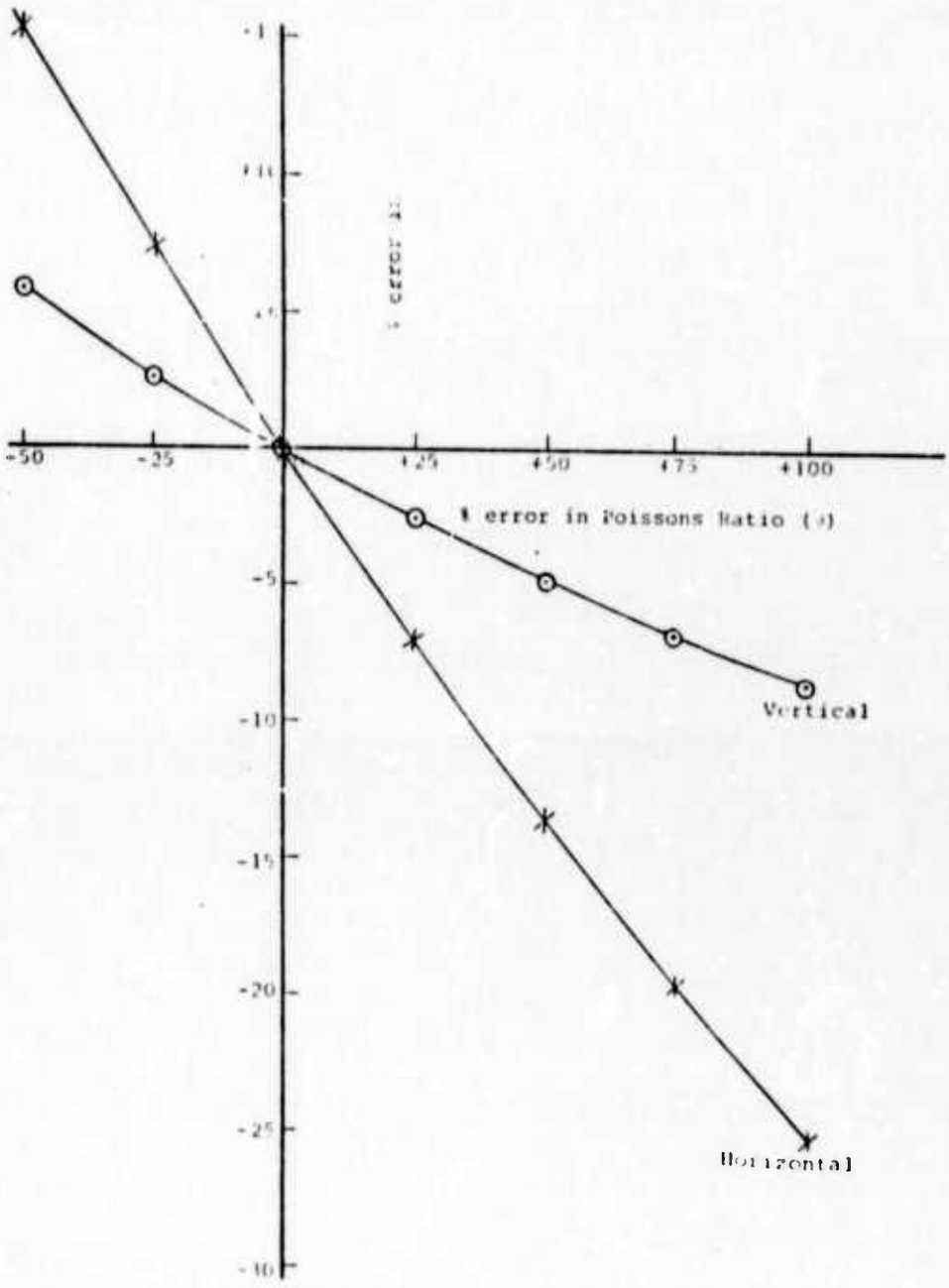

Fig.31 Sensitivity to error in Poisson's Ratio

may be possible by replacing the Kirsch solution with the solution presented by Hiramatsu and Oka (1962). Limited experimental data tends to confirm the validity of the basic approach and agrees reasonably well with the analysis in view of the potential errors in material properties used as well as experimental errors in the measured strains.

Solutions developed may be used to provide input into the design of the device. It has been shown that the ratio of strain gage grid length to trepanning hole diameter should be kept as small as possible, 2) positioning of the strain gages accurately in the pattern is essential and 3) computed stresses are directly sensitive to errors in Young's modulus of elasticity but much less sensitive to errors in Poisson's ratio.

APPENDIX

Description of Computer Programs

PROGRAM SAP

I IDENTIFICATION

SAP - Structural Analysis Program

Programmed by E. Wilson, L. Jones, H. Dovey and T. Hsueh (1970)

Program modified for use on CDC-3400 at the South Dakota School of Mines and Technology by M. Sateesha.

II PURPOSE

The purpose of this computer program is to determine nodal displacements and element stress resultants of any three dimensional solid subjected to general loading by performing linear elastic analysis. The definitions for the input and output data are given below:

III INPUT DATA

For each three-dimensional structure to be analyzed, a group of punch cards is required in this sequence.

A. TITLE CARD (12A6)

Columns 1-72 Alphanumeric title for problem identification

B. CONTROL CARD (3I5)

Columns 1-5 Number of nodal points

6-10 Number of element types

11-15 Number of load cases

C. NODAL POINT DATA CARDS (7I5,3F10.0,I5)

One card per nodal point. Nodal coordinate cards need not be in nodal order sequence. If cards are omitted the nodal data for a series of nodes is generated.

Columns 1-5	Identification - Nodal number
6-10	B.C. Code for displacement in X-direction
11-15	B.C. Code for displacement in Y-direction
16-20	B.C. Code for displacement in Z-direction
21-25	B.C. Code for rotation about X-axis
26-30	B.C. Code for rotation about Y-axis
31-35	B.C. Code for rotation about Z-axis
36-45	X-ordinate
46-55	Y-ordinate
56-65	Z-ordinate
66-70	Mesh generation parameter

A boundary condition code of zero or blank indicates that the joint is free to move in that direction and loads may be applied. A boundary condition code of one indicates that the joint is fixed in that direction.

If a particular degree of freedom is fixed for a series of cards this may be indicated by a boundary condition code of -1 on the first card in the series and +1 on the last card in the series.

D. ELEMENT DATA CONTROL CARD (4I5)

Columns 1-5 The number 5

6-10 Total number of elements

11-15 Number of different materials

16-20 Number of element distributed load sets

E. MATERIAL PROPERTY CARDS (I5,4F10.0)

Columns 1-5 Material identification number

6-15 Modulus of elasticity, E

16-25 Poisson's Ratio,

26-35 Weight density of material

36-45 Coefficient of thermal expansion

F. ELEMENT DISTRIBUTED LOAD SET CARDS (2I5,2F10.0,I5)

Columns 1-5 Load set identification number

6-10 Load type: 1 for constant surface pressure, 2 for hydrostatic pressure

11-20 Pressure for load type 1 or specific gravity for load type 2

21-30 Reference water level

31-35 Element face which pressure acts upon

G. REFERENCE TEMPERATURE (2F10.0) CARD

Columns 1-10 Stress free temperature

11-20 Acceleration due to gravity

H. ELEMENT LOAD CASE FACTOR CARDS (5 cards of 4F10.0)

Pressure and thermal load factors on the element load

cases are scaling factors in order to provide flexibility in modifying applied loads.

Card 1:	Columns 1-10	Pressure load	A
	11-20	factors for	B
	21-30	element load	C
	31-40	cases	D
Card 2:	Columns 1-10	Thermal load	A
	11-20	factors for	B
	21-30	element load	C
	31-40	cases	D
Card 3:	Columns 1-10	Percentage of gravity	A
	11-20	acting in +X	B
	21-30	direction in element	C
	31-40	load case	D
Card 4:	Columns 1-10	Percentage of gravity	A
	11-20	acting in +Y	B
	21-30	direction in element	C
	31-40	load case	D
Card 5:	Columns 1-10	Percentage of gravity	A
	11-20	acting in +Z	B
	21-30	direction in element	C
	31-40	load case	D

G. ELEMENT CARDS (12I5,4I2,2I1,F10.2)

Columns 1-5	Element number	
6-10	Global	1
11-15	node	2
16-20	point	3
21-25	numbers	4
26-30	corresponding	5
31-35	to	6
36-40	element	7
41-45	nodes -	8
46-50	Integration order	
51-55	Material number	
56-60	Generation Parameter	
61-62	Distributed load set	A
63-64	number for	B
65-66	element load cases	C
67-68	(zero implies no load)	D
69-70	Face numbers for stress output	
71-80	Element temperature	

Note: 1. Element cards must be in ascending order

2. Computation time increases with the cube of the integration order. The order is 2 for rectangular elements and 3 for skewed elements

3. Element faces are numbered as follows

Face 1 Corresponds to $+\xi$ direction

2 Corresponds to $-\xi$ direction

3 Corresponds to $+\eta$ direction

4 Corresponds to $-\eta$ direction

5 Corresponds to $+\zeta$ direction

6 Corresponds to $-\zeta$ direction

0 Corresponds to the center of the element

4. Sign convention: A positive distributed load acts in the positive (local) axis direction associated with each face.

H. CONCENTRATED LOAD DATA CARDS (2I5,6F10.0)

One card per load case for each node which has non-zero concentrated loads or moments applied. The cards must be in nodal number sequence

Columns 1-5 Nodal number

6-10 Load condition number

11-20 Load in X-direction

21-30 Load in Y-direction

31-40 Load in Z-direction

41-50 Moment about X-axis

51-60 Moment about Y-axis

61-70 Moment about Z-axis

J. BLANK CARD

The above sequence of cards must be terminated with one blank card.

K. ELEMENT LOAD MULTIPLIER CARDS (4F10.0)

One card must be supplied for each load condition which contains the following information

Columns 1-10 Multiplier for element load A

11-20 Multiplier for element load B

21-30 Multiplier for element load C

31-40 Multiplier for element load D

These cards must be in load order sequence.

IV OUTPUT INFORMATION

The program prints the following output

A. Input

B. Nodal displacements

C. Element Stresses.

PROGRAM SOLID

I IDENTIFICATION

SOLID - A modified version of SAP

Program developed for use on CDC-3400 at the South Dakota School of Mines and Technology by M. Sateesha.

II PURPOSE

The purpose of this program is to generate the element stiffness and stress matrices for eight node hexahedral three-dimensional solid elements. The definitions for the input and output data are given below.

III INPUT DATA

Same as in sections A-G as described under Program SAP.

IV OUTPUT INFORMATION

A. Element stiffness and pointer matrices on tape unit 2.

B. Element stress matrices on tape unit 8.

PROGRAM ASEMBLE

I IDENTIFICATION

ASEMBLE - Assemblage of element stiffness matrices

Programmed by M. K. Sateesha

Department of Geological Engineering

South Dakota School of Mines and Technology, Rapid City

II PURPOSE

The purpose of this computer program is to assemble the element stiffness matrices into a global stiffness matrix.

III INPUT DATA

A. DISK CONTROL CARD (2I5)

Columns 1-5 Maximum number of records on random access disk

6-10 Maximum number of rows that can be handled at a time.

B. INPUT TAPE ON UNIT 2

This tape is obtained as output from program SOLID. It contains the element stiffness and pointer matrices.

C. CONTROL CARD (2I5)

Columns 1-5 Number of equations

6-10 Number of nodes at which load boundary conditions are specified.

D. LOAD CONDITION CARDS (4I5,3F10.4)

Columns 1-5	Nodal number
6-10	B.C. Code for displacement in +X direction
11-15	B.C. Code for displacement in +Y direction
16-20	B.C. Code for displacement in +Z direction
21-30	Load in X-direction
31-40	Load in Y-direction
41-50	Load in Z-direction

IV OUTPUT INFORMATION

The program prints the input and writes the assembled stiffness matrix (global), load vector and pointer matrix on tape unit 4.

PROGRAM GSOR

I IDENTIFICATION

GSOR - Gauss-Seidel over Relaxation Technique

Programmed by M. K. Sateesha

Department of Geological Engineering

South Dakota School of Mines and

Technology, Rapid City

II PURPOSE

The purpose of this computer program is to solve a set of linear simultaneous equations utilizing the well known Gauss-Seidel iteration. The solution is refined at the end of every cycle by using an over-relaxation factor.

The program is specifically suited for banded equations since the zero coefficients are not stored and the corresponding operations skipped thus saving both storage and time.

III INPUT DATA

A. INPUT PARAMETER CARD (2I5,F10.0)

Columns 1-5 Number of equations to be solved

6-10 Maximum number of iterations

11-20 Tolerance allowed

B. INITIAL DISPLACEMENT CARDS (4E20.8) - OPTIONAL

If these cards are not provided, the initial values are all assumed to be zeros.

IV OUTPUT INFORMATION

The program prints the following output:

A. The starting displacememt values.

B. Whether the solution converged or not.

C. The number of iterations required for converging to the final solution.

D. The final solution.

PROGRAM DISTRES

I IDENTIFICATION

DISTRES - Determination of element stresses and strains

Programmed by Malalur K. Sateesha

Department of Geological Engineering

South Dakota School of Mines and Technology, Rapid City

II PURPOSE

The purpose of this program is to compute the element stresses and strains from the nodal displacements.

III INPUT DATA

A. TITLE CARD (12A6)

Columns 1-72 Alphanumeric title for problem identification

B. CONTROL CARD (2I5)

Columns 1-5 Number of nodal points

6-10 Number of element types

C. MATERIAL PROPERTY CARD (2F10.0)

Columns 1-10 Young's Modulus

11-20 Poisson's Ratio

D. NODAL DISPLACEMENT CARDS (4E20.8)

These cards are obtained as output from Program GSOR.

E. TAPE UNIT 1 - OUTPUT TAPE UNIT 8 FROM PROGRAM SOLID

III OUTPUT INFORMATION

1. Input Data
2. Nodal Displacements
3. Element Stress Resultants
4. Element Strain Resultants

PROGRAM PRIN

I IDENTIFICATION

PRIN - Principal Stress Determination Program

II PURPOSE

The purpose of this computer program is to determine the principal stresses and their directional cosines for any given stress tensor.

III INPUT DATA (3 cards of 3F20.8)

The stress tensor is read rowwise and stored as

$$\begin{matrix} \sigma_x & \tau_{xy} & \tau_{xz} \\ \tau_{xx} & \sigma_y & \tau_{xz} \\ \tau_{zx} & \tau_{zy} & \sigma_z \end{matrix}$$

IV OUTPUT INFORMATION

The principal stresses are obtained as

$$\begin{matrix} \sigma_1 & 0 & 0 \\ 0 & \sigma_2 & 0 \\ 0 & 0 & \sigma_3 \end{matrix}$$

and the directional cosines as

$$\begin{matrix} V1\text{-}X & V2\text{-}X & V3\text{-}X \\ V1\text{-}Y & V2\text{-}Y & V3\text{-}Y \\ V1\text{-}Z & V2\text{-}Z & V3\text{-}Z \end{matrix}$$

where

V1, V2, V3 = Unit vectors along directions σ_1, σ_2, and σ_3 respectively.

and

X, Y, Z = components of the vectors along the Global

coordinate directions.

LIST OF REFERENCES

ARGYRIS, J.H., 1955, Energy Theorems and Structural Analysis, Aircraft Engineering, v. 27, p. 125-154.

CLOUGH, R.W., 1965, The Finite Element Method in Structural Mechanics, Stress Analysis (Ed. Zienziewicz and Hollister). John Wiley and Sons, New York, Chap. 7, p. 85-119.

DANIELLS, P., 1971, Experimental Measurement of Residual Strain in Rocks, M.S. Thesis, S.D. School of Mines and Technology, Rapid City.

EMERY, C.L., 1964, "Strain Energy in Rocks," State Of Stress in Earth's Crust, American Elsevier, New York, pp. 234-279.

FELIPPA, C.A. and CLOUGH, R.W., 1970, The Finite Element Method in Solid Mechanics, Numerical Solution of Field Problems in Continuum Physics, SIAM-AMS Proc., v. II, Amer. Math. Soc., Providence, Rhode Island.

FRIEDMAN, M., 1968, "X-ray Analysis of Residual Elastic Strains in Quartzose Rocks": Tenth Sym. on Rock Mech., (in press), Austin, Texas.

GOLDICH, S.S. et.al., 1961, The Precambrian Geology and Geochronology of Minnesota, Minnesota Geological Survey Bull., 41, Minneapolis, 193 p.

HAFNER, W., 1951, Stress Distribution and Faulting, Geol. Soc. America Bull., v. 62, p. 373-398.

HAIMSON, B., 1973, Real Stresses Around Boreholes, Proceedings of the Sixth Conference on Drilling and Rock Mechanics, The University of Texas, Austin, Texas.

HAIMSON, B., LaCOMB, J., JONES, A.H., and GREEN, S.J., 1974, Crustal Stresses At The Nevada Test Site, Transaction of The A.G.U., vol. 55, no. 4, p. 425.

HALL, 1899, The Gneisses, Gabbros, Schist and Associated Rocks of Southwestern Minnesota, USGS Bull, 157.

HEALY, J.H., ROLLER, J.C., GORTON, Q., and LAMSON, R. 1974, In Situ Stress Measurements in Fractured Rocks, Transactions of the A.G.U., vol. 55, no. 4, p. 425

HIRAMATSU, Y. and OKA, Y., 1962, Stress Around a Shaft or Level Excavated in Ground with a Three Dimensional Stress State, Faculty of Engineering Memoirs, Kyoto University, Japan, 24.

HOSKINS, E., 1967, An Investigation of Strain Rosette Relief Methods of Measuring Rock Stress, Int. J. Rock Mech. Min. Sci., v. 4, p. 155-164.

HOSKINS, E., 1968, A Stress Measurement Technique for Deep Holes, Trans. AGU,v. 49, no. 4, p. 756.

HOWARD, J.H., 1966, Structural Development of the Williams Range Thrust, Colorado, Geol. Soc. America Bull., v. 77 p. 1247-1264.

HOWLAND, R.C.J., 1930 On the Stresses in The Neighborhood of a Circular Hole on a Strip Under Tension, Phil. Trans., Roy. Soc. (London), Series A. v. 229, p. 49-86.

KEHLE, R.O., 1964, Determination of Tectonic Stresses Through Analysis of Hydraulic Well Fracturing, J. Geoph. Res., v. 69. p. 259-273.

KIRSCH., G. 1898, "Die Theorie der Elastizitat und die Bedurfnisse der Festigkeitslehre," Zeitschrift Verein Deutscher Ingenieure: vol. 42, no. 29 pp. 797-807.

McCLINTOCK, F.A. and ARGON, A.S., 1966 Mechanical Behavior of Materials, Addison-Wesley Pub. Co., Reading, Pa.

PRZEMIENIECKI, J.S., 1968, Theory of Matrix Structural Analysis, McGraw Hill Book Co., New York, 468 p.

SANFORD, A.R., 1959, Analytical and Experimental Study of Simple Geologic Structures, Geol. Soc. America Bull.,v. 70, p. 19-52.

SATEESHA, M.K., 1974, "Analysis of Data from a Deep Hole Stress Measurement Device," Ph.D. thesis, S.D. School of Mines and Technology.

SOETE, W. and VANCROMBRUGGE, R., 1950, "An Industrial Method for the Determination of Residual Stresses," Proc. - Society for Experimental Stress Analysis, vol. 8, no. 1, pp. 17-28.

THEIL, G.A. and DUTTON, C.E., 1935, The Architectural, Structural and Monumental Stones of Minnesota, Minnesota Geol. Survey, Bulletin No. 25, Minneapolis, p. 160.

VARNES, D.J., 1969, "Model for Simulation of Residual Stress in Rock," Rock Mechanics-Theory and Practice, Proc. Eleventh Sym. on Rock Mech., AIME, New York, pp. 415-426.

WHITE, JON, 1973, Effects of Small Temperature Changes on Measured Apparent Residual Strain in Selected Rock Cylinders, M.S. Thesis, South Dakota School of Mines and Technology, Rapid City, South Dakota.

ZIENKIEWICZ, O., 1971, The Finite Element Methods in Engineering Science, McGraw Hill Book Co., London, p. 521.